

Two-population Bayesian hierarchical model of type Ia supernovae

Radosław Wojtak^{1*}, Jens Hjorth¹, Jacob Osman Hjortlund¹

¹*DARK, Niels Bohr Institute, University of Copenhagen, Jagtvej 128, 2200 Copenhagen, Denmark*

29 August 2023

ABSTRACT

The currently used standardisation of type Ia supernovae results in Hubble residuals whose physical origin is unaccounted for. Here, we present a complete physical interpretation of the Hubble residuals based on a novel Bayesian hierarchical model of type Ia supernovae in which latent variables describing intrinsic and extrinsic (dust related) supernova properties originate from two supernova populations. Fitting the model to SALT2 light curve parameters of supernovae in the Hubble flow we find strong (4σ) evidence for the presence of two overlapping, but distinct, populations differentiated primarily by their mean SALT2 shape parameter (stretch) x_1 . Supernovae from the population with predominantly slow decliners (higher average x_1) are found to be intrinsically bluer (mean SALT2 colour $c \approx -0.11$) and twice as reddened by dust (mean reddening $E(B - V) \approx 0.10$) than those from the other population which is dominated by fast decliners (lower average x_1) with $c \approx -0.04$ and $E(B - V) \approx 0.05$. The inferred extinction coefficient R_B in both supernova populations follows a broad distribution (scatter 0.9) with a mean of 4.1, which coincides closely with the value associated with mean extinction law in the Milky Way. We also find that the supernova data favour a peaked (two-tailed) distribution of selective extinction $E(B - V)$ over the commonly adopted exponential model. Our approach provides a complete explanation of the distribution of supernova light curve parameters in terms of extinction properties and the above-mentioned differences between the two populations, without the need for introducing any intrinsic scatter.

Key words: cosmology: observations – cosmology: distance scale – transients: supernovae – methods: statistical

1 INTRODUCTION

Type Ia supernovae serve as one of the primary probes of cosmological models. They were a cornerstone of the discovery of cosmic acceleration (Riess et al. 1998; Perlmutter et al. 1999) followed by establishing the standard Λ CDM cosmological model. Today, they are used to produce some of the leading data sets to constrain the dark energy equation of state (Brout et al. 2022a; Jones et al. 2019) and play a key role in high precision determinations of the Hubble constant (Riess et al. 2022; Freedman et al. 2019). Type Ia supernovae will also be one of the major drivers of future cosmological tests based on observations from massive sky surveys conducted with next-generation telescopes such as the Vera C. Rubin Observatory (LSST Science Collaboration et al. 2009) and the *Nancy Grace Roman Space Telescope* (Wang et al. 2022).

The key element of type Ia supernova analysis is a process of standardisation whose goal is to improve the precision of distance measurements by means of applying empirical corrections based on observationally determined correlations between supernova apparent magnitudes and selected properties of their light curves. The standard approach accounts for corrections in two well measurable observables: the rest-frame width of the light curve (hereafter stretch parameter) and the apparent colour at a fixed phase of the light curve (typically at the peak of the light curve). The corrections are purely empirical with all relevant coefficients measured directly from data. This strategy was proposed a few decades ago by Tripp (1998) and since then it has been used in virtually all cosmological analyses with type Ia supernovae.

The stretch correction was first established by Phillips et al. (1999). Kasen & Woosley (2007) showed that the correction most likely reflects an underlying relation between the the mass of radioactive ^{56}Ni synthesised in the supernova explosion, which is the primary determinant of the super-

* E-mail: radek.wojtak@nbi.ku.dk

nova peak bolometric luminosity (Arnett 1982), and broad absorption features developed after the peak and dominating in the B -band, although a possible modulation by the total ejected mass and its relation to the progenitor may complicate this picture (Scalzo et al. 2014a,b).

The physical nature of the colour correction is quite different. The correction is a hybrid term which mixes possible effects related to supernova intrinsic colours, which may vary across supernovae and their progenitors, and dust reddening which is naturally expected to vary across supernova host galaxies and local environments. Many attempts to disentangle supernova intrinsic colours from the effect of dust have led to independent estimates of the extinction coefficient $R_B = A_B/E(B - V)$, i.e. the ratio of total A_B to selective $E(B - V)$ dust extinction in the B -band. The results point to extremely low values ($R_B \lesssim 3$; see e.g. Nobili & Goobar 2008; Cikota et al. 2016; Wang et al. 2008; Hicken et al. 2009) relative to average $R_B = 4.3$ measured in the Milky Way (Schlafly et al. 2016) and $R_B = 3.8$ estimated in external galaxies (Finkelman et al. 2010). This apparent discrepancy is a long-lasting problem and it signifies that either there are special low-extinction conditions operating solely in supernova sight lines (see e.g. Goobar 2008; Bulla et al. 2018) or the measurements of extinction from supernova observations need to be revised with more accurate models (Mandel et al. 2017).

The standard two-parameter correction of supernova peak magnitudes (hereafter the Tripp calibration after Tripp 1998) gives rise to irreducible intrinsic scatter in the Hubble residuals. The intrinsic scatter is a well measured property of the supernova Hubble diagrams and is typically found to be $\gtrsim 0.1$ mag with minor improvements from applying phenomenological second-order corrections such as a step function in the host stellar mass (Kelly et al. 2010; Scolnic et al. 2018; Jones et al. 2019; Smith et al. 2020) or the local specific star formation rate (Rigault et al. 2020). Inevitably, it is also a standard nuisance parameter in cosmological analyses of type Ia supernovae where it is one of the main sources of the total uncertainty in supernova distance moduli.

The persistence of a non-vanishing intrinsic scatter could be regarded as a sign that the Tripp calibration provides an incomplete framework for modelling type Ia supernovae. The argument is two-fold. Firstly, intrinsic scatter in its simplest form does not account for a range of second-order effects in the distribution of the Hubble residuals. Examples include an excess of positive residuals in red supernovae from low-mass host galaxies and a trend of the intrinsic scatter increasing with supernova colour (larger scatter in redder supernovae; Brout & Scolnic 2021; Popovic et al. 2021). Substantial differences between the Hubble residual distributions are also apparent when comparing the calibration sample (host galaxies with distances calibrated with Cepheids) and the Hubble flow sample of type Ia supernovae used in the local determination of the Hubble constant (Wojtak & Hjorth 2022). Secondly, intrinsic scatter as such is naturally expected to result from neglecting a range of latent variables. Understanding the physical origin of the Hubble residuals and the intrinsic scatter should be imperative not only for the reason of developing models which are more rooted in first principles, but also for the sake of eliminating potential biases in cosmological measurements arising from unaccounted for supernovae properties.

Cosmological biases may occur, for example, when one neglects the observationally permissible scenario in which type Ia supernovae originate from two populations of progenitors, tracing old and young stellar populations, respectively (Rigault et al. 2020). The bias in this case would be a direct consequence of ignoring the redshift dependence of the population weights regulated by the star formation history.

Recent developments of Bayesian hierarchical models of type Ia supernovae operating at the level of light curve parameters (see e.g. Mandel et al. 2017; Brout & Scolnic 2021; Popovic et al. 2021) or spectral energy distributions as light curve fitters (Mandel et al. 2022) have helped pin down the physical cause of a substantial fraction of the intrinsic scatter in supernova Hubble diagrams. With physically motivated priors for dust reddening, models can disentangle in a probabilistic way the effect of dust from supernova intrinsic colours. Analyses of several different supernova samples concluded consistently that excessive and asymmetric Hubble residuals in red supernovae can be attributed to a wide range of extinction coefficients (Thorp et al. 2021; Brout & Scolnic 2021). The implied distributions of R_B overlap substantially with those known from the Milky Way (Fitzpatrick 1999; Schlafly et al. 2016), although they tend to peak at slightly lower values: $R_B \approx 3.8$ (Mandel et al. 2017; Thorp et al. 2021) relative to $R_B \approx 4.3$ measured in the Milky Way (Schlafly et al. 2016). The implied dust model leads to a reduction of the intrinsic scatter by about 40 per cent (Thorp et al. 2021; Mandel et al. 2022). Brout & Scolnic (2021) showed that further reduction is possible when extinction properties are inferred independently in two bins of supernova host galaxies split by the stellar mass with respect to the transition mass of the mass step correction, i.e. $10^{10} M_\odot$ (although see Uddin et al. 2020). This analysis implies very low values of the extinction coefficient in more massive host galaxies with respect to the Milky Way ($R_B \approx 2.5$ compared to $R_B \approx 4.3$ from Schlafly et al. 2016). This result begs the question what physical mechanisms can form dust with this extinction property and why they are efficient only in host galaxies with stellar masses larger than $10^{10} M_\odot$.

One limitation of the currently proposed Bayesian hierarchical models of type Ia supernovae is the assumption that type Ia supernovae form a single population whose intrinsic and extrinsic properties are drawn from unimodal prior distributions. This assumption can hardly be reconciled with observations which provide evidence for the existence of two supernova populations distinguished by the decline rate of their light curves and the stellar age of their environments (Rigault et al. 2013, 2020; Maoz et al. 2014). Fast declining supernovae are typically found in old stellar populations, while slowly declining supernovae originate in young star forming environments (Sullivan et al. 2006). Both supernova populations exhibit slightly different normalisation of their Hubble diagrams and when taken into account in the standardisation, this property can effectively reduce the intrinsic scatter (Rigault et al. 2020). This suggests that the notion of two supernova populations should be regarded as a potentially important element of a model explaining the Hubble residuals and perhaps a missing element of the present Bayesian hierarchical models. The two observationally distinguished populations linked to young and old

stellar environments likely originate from different progenitor channels. Based on an argument of time scales between the formation of a binary system and the supernova explosion, it is tempting to associate progenitors of supernovae in young (old) stellar populations with single-degenerate (double-degenerate) systems (Maoz et al. 2014). The two progenitor channels would manifest themselves as prompt (short time scale) and delayed (long time scale) supernovae whose rates follow the star formation history (prompt) or are lagging behind (delayed) with the delay time following the distribution $\propto t^{-1}$ expected for double degenerate progenitors. Measurements of the type Ia supernova rate as a function of redshift or galaxy properties are consistent with the presence of both prompt and delayed supernova populations (Scannapieco & Bildsten 2005; Mannucci et al. 2006; Rodney et al. 2014; Andersen & Hjorth 2018). Although the two-channel scenario is commonly accepted as a framework for studying supernova progenitors, we emphasise that its status should be regarded as a working hypothesis rather than a fully confirmed theory (Livio & Mazzali 2018).

The goal of our study is to incorporate the notion of two supernova populations (with no prior assumptions on their physical properties) in a Bayesian hierarchical model of type Ia supernova light curve parameters. We aim to demonstrate that including this observationally motivated assumption enables us to fully account for the intrinsic scatter resulting from the Tripp calibration in terms of effects of dust and differences between the physical properties of two supernova populations separated probabilistically by the new model. Using a data-driven approach we also improve the prior for the distribution of dust reddening adopted in previous studies. This prior distribution is the key element of disentangling dust reddening from supernova intrinsic colour in the Bayesian hierarchical modelling.

An important motivation for developing the model is to prepare the ground for a physical interpretation of the recently found intrinsic tension in the supernova sector of the local determination of the Hubble constant with distances calibrated with Cepheids (Wojtak & Hjorth 2022). The tension arises as a discrepancy between the colour corrections of type Ia supernovae in the calibration sample (host galaxies with independently observed Cepheids) and the Hubble flow, with (only) the former being entirely consistent with a typical extinction correction in the Milky Way. This represents an intrinsic anomaly of the Tripp calibration, which assumes universality of the colour correction across all supernova samples, and thus a potential source of unaccounted systematic errors in the local measurement of the Hubble constant from the Supernovae and H_0 for the Dark Energy Equation of State (SH0ES) program (Riess et al. 2016, 2019, 2021). Since host galaxies in the calibration sample are selected as late type galaxies containing observable Cepheids, it is natural to investigate if the different supernova colour corrections in these samples reflect a different mixture of supernova populations (perhaps dominated by one of them) and extinction in the underlying young stellar environments in the calibration sample vs. the host galaxies of the Hubble flow. Although selecting similar late-type galaxies in the Hubble flow as in the calibration sample has a negligible impact in the Hubble constant determination (Riess et al. 2022), it is imperative to check whether other approaches can corroborate this conclusion or not. Unlike the strategy

based on matching galaxy properties on the two rungs of the distance ladder, Bayesian modelling of supernova light curve parameters is capable of measuring probabilistic properties of extinction in sight lines towards observed supernovae. We expect that the model developed in our work will shed more light on this problem and its impact on the Hubble constant determination.

The outline of the paper is as follows. In section 2 we describe the model including an implementation of the two-population assumption, the adopted hyperpriors and the related hyperparameters as well as the inference method. The supernova data and the results of fitting several different versions of the model are presented in section 3. In this section we also demonstrate the completeness and accuracy of the final model in terms of accounting for supernova Hubble residuals from the Tripp calibration. In section 4 we discuss the implied intrinsic properties of supernovae and extrinsic properties of dust in the context of ongoing type Ia supernova studies. We summarise our findings in section 5.

2 MODEL

2.1 Rationale

The multi-band light curve of a normal type Ia supernova can be effectively described by three parameters: the peak magnitude, the rest-frame width of the light curve, and the apparent colour. These parameters can be measured directly from observations by fitting empirical models of multi-band light curves generated from spectral templates obtained for a large number of supernovae. One can think of light curve parameters as a minimum set of observables describing a normal type Ia supernova light curve without loss of information (maximum data compression). In this study, we use parameters obtained with the SALT2 light curve fitter (Betoule et al. 2014): light curve amplitude quantified by the apparent B -band peak magnitude in the supernova rest frame m_B , the dimensionless parameter x_1 describing the light curve stretch, and the colour parameter c describing the restframe $B - V$ colour at restframe B -band peak.

Light curve parameters only provide a phenomenological description of the observed supernova light curves. Their relation to the corresponding intrinsic (e.g. intrinsic supernova colour) and extrinsic (e.g. dust reddening and extinction) physical parameters is highly degenerate due to the fact that the number of relevant latent variables is typically larger than the number of light curve parameters. This problem is immediately apparent taking as an example the supernova colour: while a single parameter suffices to describe the apparent supernova colours, the actual physical parameters needed to explain them include intrinsic colours related to the physics of supernova explosions and initial conditions, and reddening due to dust in the host galaxy. Although most of the physical parameters cannot be directly inferred from observed light curves due to the above-mentioned degeneracy, they do shape the distribution of directly measured light curve parameters. Therefore, modelling the distribution of light curve parameters can be used to determine statistical properties of latent physical parameters for a given supernova population. This inference is a standard problem which can be handled using Bayesian hierarchical modelling.

As a starting point for Bayesian hierarchical modelling we formulate relations between observables and latent variables. We adopt a commonly used model which enables us to separate intrinsic supernova properties from extrinsic effects related to dust reddening and extinction (see e.g. Mandel et al. 2017; Brout & Scolnic 2021). The model quantifies the intrinsic properties in terms of the absolute peak magnitude M_B , the stretch parameter X_1 (assumed to be equal to the stretch parameter x_1 from SALT2 and distinguished from it only for the sake of concise mathematical formulation below), the intrinsic $B-V$ colour c_{int} at the light curve maximum as well as empirical coefficients of possible relations between m_B and $\{X_1, c_{\text{int}}\}$. The intrinsic parameters only provide a phenomenological description of physical processes behind the observed supernova light curves. However, they can be directly linked to initial conditions of type Ia supernovae given a complete physical model of supernova explosions. The extrinsic latent variables include dust reddening $E(B-V)$ and extinction coefficient R_B .

The model relating the latent variables to the measured light curve parameters is given by the following equations:

$$\begin{aligned} m_B &= M_B - \alpha X_1 + \beta c_{\text{int}} + \mu(z) + R_B E(B-V) \\ x_1 &= X_1 \\ c &= c_{\text{int}} + E(B-V), \end{aligned} \quad (1)$$

where $\mu(z)$ is the distance modulus and z is the CMB rest frame redshift of the supernova. It can be thought of as the simplest generalisation of the Tripp calibration (Tripp 1998) which can be recovered when the effect of extinction and intrinsic colour correction are indistinguishable, i.e. $\beta = R_B$. For the sake of simplicity, we will hereafter refer to all variables and coefficients on the right hand side of the equations as a latent variable vector ϕ , i.e. $\phi = \{M_B, X_1, c_{\text{int}}, E(B-V), \alpha, \beta, R_B\}$, and to those on the left hand side as observables $\xi = \{m_B, x_1, c\}$.

2.2 Two-population model

Observations provide evidence that type Ia supernovae with fast or slowly declining light curves (low or high stretch parameter) originate from passive and star-forming environments, respectively (Sullivan et al. 2006; Rigault et al. 2013, 2020; Larison et al. 2023). The corresponding supernova populations can be identified probabilistically as two components in the distribution of stretch parameters. A bimodal distribution of stretch parameter signifying the presence of two supernova populations is apparent in many low-redshift supernova compilations (Scolnic & Kessler 2016; Scolnic et al. 2018; Dhawan et al. 2022) and volume limited samples at high redshifts (Nicolas et al. 2021). We incorporate this observational fact in our model by introducing two separate supernova populations for which prior distributions of latent variables can differ. We assume that possible differences between prior distributions of the two populations may occur in variables associated with intrinsic and extrinsic properties. Differences between intrinsic properties may reflect two sets of initial conditions in the two supernova populations, which may in turn be related to the progenitor channels. Analogous differences in the dust sector can arise from diverse conditions of supernova local environments and lines of sight. They can potentially reflect diverse dust prop-

erties in star-forming and passive environments traced by the two supernova populations.

We employ a two-population model in a probabilistic way by introducing a prior probability w that a given supernova originates from one of the two supernova populations. The prior probability regulates the ratios of supernova populations in a given sample so that the probability of observing a supernova with latent (physical) parameters ϕ is given by

$$p(\phi) = wp_{\text{prior}1}(\phi) + (1-w)p_{\text{prior}2}(\phi), \quad (2)$$

where $p_{\text{prior}i}$ is the prior probability distribution of latent variables in the i -th supernova population. Once the prior probabilities in the two populations are known one can determine the distribution of observables ξ_0 as

$$p(\xi_0) = \int \delta(\xi_0 - \xi(\phi)) [wp_{\text{prior}1}(\phi) + (1-w)p_{\text{prior}2}(\phi)] d\phi, \quad (3)$$

where $\xi(\phi)$ is given by eqs. (1) and the integral over latent variables can be effectively computed in a Monte Carlo way by sampling from the prior distributions of the two supernova populations. We will use this equation to show a quantitative interpretation of well studied residuals in Hubble diagrams of type Ia supernova standardised with the Tripp calibration (Tripp 1998).

We constrain the prior weight w and the properties of the resulting populations solely from the supernova data. The two populations are disentangled probabilistically through correlated signatures of two distinct components in the distributions of the latent variables. As shown by Rigault et al. (2020) and Nicolas et al. (2021), type Ia supernovae with slowly or fast declining light curves (positive or negative x_1) can be differentiated not only by the local specific star formation rate of their environments but also as two separable components of the stretch parameter distribution. It is perhaps not surprising that the two supernova populations emerging in our model are primarily distinguished by their mean stretch parameters and represent fast and slowly declining supernovae. What is unique in our model is that it enables us to quantify which remaining intrinsic and extrinsic properties are common to the both populations and which are different.

2.3 Priors

We assume that all latent variables except for α , β and $E(B-V)$ follow independent Gaussian distributions. The corresponding means and standard deviations are free parameters (hyperparameters) to be constrained by observations. We assume that both α and β are single-valued parameters with the corresponding distributions given by δ functions.

The selective extinction $E(B-V)$ is a positively defined variable. This is a strict physical condition which narrows down a range of possible prior distributions. In our model we adopt a flexible two-parameter family of probability distributions given by the gamma distribution:

$$p_{\text{prior}}(y = E(B-V)/\tau) = \frac{y^{\gamma-1} \exp(-y)}{\Gamma(\gamma)}. \quad (4)$$

The assumed class of probability distributions is the maximum information entropy solution (the most likely function)

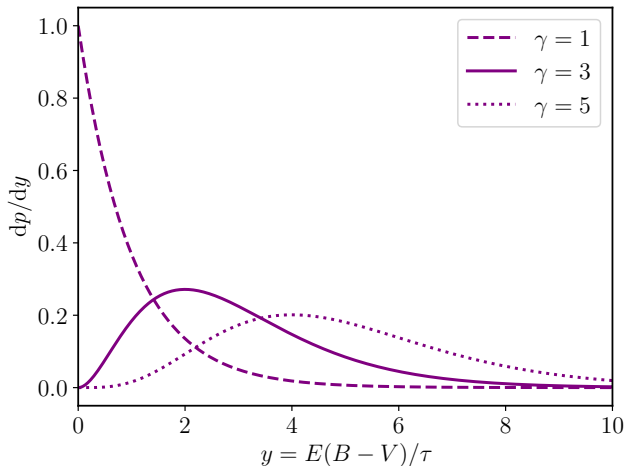


Figure 1. The prior probability distribution of $y = E(B - V)/\tau$ for a range of shape parameter values, plotted up to the adopted upper limit $y_{\max} = 10$.

for a positively defined variable subject to constrained mean values of the variable and its logarithmic counterpart. The free parameters describe the shape of the distribution (α) and a characteristic scale of the most probable values (τ). The gamma distribution reduces to an exponential model when $\gamma = 1$. All distributions with $\gamma > 1$ are peaked at $y > 0$ (two-tailed distributions), while the exponential case is represented by one-tailed distributions with maximum at $y = 0$. In order to control the accuracy of numerical integration over $y = E(B - V)/\tau$ in the likelihood evaluation (see the following sections and Appendix A), we cut off the distribution’s upper tail at $y_{\max} = 10$ and use the resulting renormalized truncated distributions. Figure 1 shows examples of the prior distribution plotted between $y = 0$ and y_{\max} for a range of shape parameter values.

Our choice of the prior distribution of dust reddening generalises the commonly used exponential model which is adopted in virtually all Bayesian hierarchical models from the literature (see e.g. Mandel et al. 2017, 2022; Popovic et al. 2021; Brout & Scolnic 2021). The generalisation can be justified in a two-fold way. From a statistical point of view, the choice of maximum entropy solution and the corresponding parameterization should be adjusted to the constraining power of the data in a way that there is adequate correspondence between the information capacity of the model and the actual information in the data. Unlike previous studies, we adopt equal numbers of hyperparameters (degrees of freedom) in each of the two prior distributions relevant in modelling the distribution of apparent colours: $p(c_{\text{int}})$ and $p(E(B - V))$. As we shall see in the following section, the shape parameter γ of the prior distribution of dust reddening is not a redundant parameter and it appears to be equally well constrained by the supernova data as other hyperparameters. The second argument involves basic considerations of possible geometric configurations of supernovae and intervening dust in a typical supernova host galaxy. For a randomly distributed dust clouds and supernova locations, it is natural to expect that the most probable configuration occurs for some finite column density of dust and the corresponding reddening. This configuration can be easily recon-

ciled with the gamma distribution model for which the maximum probability position is directly related to the shape parameter γ (the larger γ , the larger shift of the distribution’s peak). The exponential model does not have this flexibility and sets the maximum probability at $E(B - V) = 0$.

For the remaining parameter of the dust sector, i.e., the extinction coefficient R_B , we assume a Gaussian prior distribution. We do not apply any truncation which could exclude R_B values which are not allowed on the grounds of theoretical dust models. However, as we shall see in the following section, only low 2σ limits of our best fit models are comparable to the lower limit expected for Rayleigh scattering ($R_B = 2.2$; Draine 2003) and well above $R_B = 1.5$ adopted as a more liberal limit in analyses similar to ours (Brout & Scolnic 2021; Thorp et al. 2021). This leaves only 1–2 per cent of the lowest R_B values below theoretical limits. This fraction is sufficiently small to conclude that neglecting any truncation in the prior distribution of R_B has a negligible impact on the final results.

The distance modulus latent variable in eqs. (1) is assumed to have a Gaussian distribution. The mean value is computed for the Planck cosmological model (Planck Collaboration et al. 2020) with the Hubble constant renormalised to $H_0 = 70 \text{ km s}^{-1} \text{ Mpc}^{-1}$. Since we fit our model to supernovae in a redshift range of the Hubble flow (see more details in the following section), the assumption of a cosmological model does not have any noticeable impact on the final results and the adopted Hubble constant fixes a reference value for the absolute magnitudes. The main source of uncertainties in $\mu(z)$ comes from unconstrained peculiar velocities in the local volume. This results in the following standard deviation

$$\sigma_\mu = \frac{5}{\ln 10} \frac{\sigma_v}{cz}, \quad (5)$$

where $\sigma_v = 250 \text{ km s}^{-1}$ is a commonly adopted value of the line-of-sight peculiar velocity dispersion assumed in cosmological fits with type Ia supernovae (Scolnic et al. 2018) and equal to an upper limit of scatter in peculiar velocities with respect to the linear velocity field (Carrick et al. 2015).

All hyperparameter names are listed in Table 1. We use an intuitive notation in which \hat{X} and σ_X are used to refer to the mean and standard deviation of the corresponding latent variable X . For the sake of simplicity, we keep the same names of single-value parameter as their corresponding latent variables. We use a distinct name for the standard deviation of M_B . This parameter is a direct Bayesian counterpart of the commonly used ‘intrinsic scatter’ which quantifies excessive (unaccounted for by the model) residuals in supernova Hubble diagrams. For this reason, we label it σ_{int} .

2.4 Likelihood and inference

We constrain free hyperparameters by fitting the model to supernova data in the form of measured light curve parameters $\xi_{\text{obs},i}$, the corresponding covariance matrix $C_{\text{obs},i}$ and redshift z_i . The likelihood used in our analysis is given by the following equation

$$L \propto \prod_i^N p(\{\Theta, w\} | \xi_{\text{obs},i}, C_{\text{obs},i}, z_i), \quad (6)$$

latent variable	prior	hyperparameters [hyperpriors]
M_B	$\mathcal{G}(M_B; \widehat{M}_B, \sigma_{\text{int}})$	$\widehat{M}_B[-\infty, +\infty], \sigma_{\text{int}}[0, +\infty]$
X_1	$\mathcal{G}(X_1; \widehat{x}_1, \sigma_{x_1})$	$\widehat{x}_1[-\infty, +\infty], \sigma_{x_1}[0, +\infty]$
c_{int}	$\mathcal{G}(c_{\text{int}}; \widehat{c}_{\text{int}}, \sigma_{c_{\text{int}}})$	$\widehat{c}_{\text{int}}[-\infty, +\infty], \sigma_{c_{\text{int}}}[0, +\infty]$
α	$\delta(x - \alpha)$	$\alpha[-\infty, +\infty]$
β	$\delta(x - \beta)$	$\beta[1, 5]$
$E(B - V)$	$\propto x^{\gamma-1} \exp(-x/\tau)$	$\tau[0, +\infty], \gamma[1, 7]$
R_B	$\mathcal{G}(R_B; \widehat{R}_B, \sigma_{R_B})$	$\widehat{R}_B[1.5, 6], \sigma_{R_B}[0, 1.5]$

Table 1. Prior probability distributions of all latent variables and the corresponding hyperparameters. Each set of hyperparameters can be different in two supernova populations of the model. The last column lists all hyperparameters associated with a given prior distribution and the corresponding ranges of allowed values (flat hyperpriors). $\mathcal{G}(x; \mu, \sigma)$ denotes a normal distribution with mean μ and standard deviation σ , and $\delta(x - x_0)$ is the Dirac delta distribution.

where Θ is a vector of all hyperparameters in both supernova populations, N is the number of supernovae and probability distribution p is calculated by marginalising the product of the Gaussian probability distribution accounting for measurement uncertainties and the prior probability given by eq. (2) over all latent variables, i.e.

$$p(\{\Theta, w\} | \xi_{\text{obs } i}, \mathbf{C}_{\text{obs } i}, z_i) = \int \mathcal{G}[\xi(\phi); \xi_{\text{obs } i}, \mathbf{C}_{\text{obs } i}] p_{\text{prior}}(\phi) d\phi. \quad (7)$$

Integration over the latent variables which have Gaussian prior distributions and occur as linear terms in the model of observables, i.e. $\{M_B, x_1, c_{\text{int}}, \mu, R_B\}$, results in a sum of two Gaussian distributions weighted by w and $(1 - w)$. Integration over the remaining variable $E(B - V)$ does not have an analytical solution and thus it is carried out numerically. Therefore, each evaluation of the likelihood involves N numerical integrations over $E(B - V)$. We outline all necessary details including explicit forms of the covariance matrices resulting from the analytical part of the marginalisation in Appendix A.

We compute best fit parameters by means of integrating the posterior probability using a *Monte Carlo Markov Chain* technique implemented in the *emcee* code (Foreman-Mackey et al. 2013). For most of the hyperparameters we employ rather unrestrictive priors. In order to reduce the level of a lower tail of the prior distribution at $R_B \lesssim 1.5$ to less than 2σ , we restrict the range of σ_{R_B} to $[0, 1.5]$. We also use finite limits of hyperpriors for \widehat{R}_B , β and γ . For the mean extinction coefficient \widehat{R}_B , we adopt the bounds given by a conservative theoretical lower limit of 1.5 (Brout & Scolnic 2021; Thorp et al. 2021) and a maximum value of extinction ($R_B \approx 6$) measured in the Milky Way by Fitzpatrick & Massa (2007). Exact limits of all hyperpriors are provided in Table 1. In all cases, the adopted hyperpriors are wider than the lower and upper limits inferred from the likelihood and the main reason of using them is to stabilise convergence of the chains. For the same reason, we restrict the range of parameter w to $[0.1, 0.9]$. This prevents the chains from populating models with $w \approx 0$ or $w \approx 1$ where hyperparameters of a zero-weighted supernova population loses any constraints and its hyperparameters can diverge from the equilibrium solution. As we shall see in the following section, the adopted prior for w is wider than the actual

limits from the likelihood and thus it has no impact on the final results. Unless explicitly stated, best-fit parameters are provided in the form of posterior means and errors are computed as 16th and 84th percentiles of the marginalised probability distributions. The 1σ and 2σ confidence contours in all figures contain 68 and 95 per cent of the corresponding 2-dimensional marginalised probability distributions.

3 OBSERVATIONAL CONSTRAINTS

3.1 Observations

We use type Ia supernova light curve parameters from the *SuperCal* compilation (Scolnic et al. 2015). The supernova sample was compiled from several different surveys using a consistent photometric calibration based on Pan-STARRS observations. Supernovae in the Hubble flow were used in measurements of the Hubble constant presented in Riess et al. (2016, 2019, 2021) based on consecutive improvements of distance anchors. The compilation provides best fit light curve parameters of the SALT2 model (Betoule et al. 2014): the apparent B -band peak magnitude in the supernova rest frame m_B , dimensionless parameter x_1 describing the light curve shape (stretch parameter) and colour parameter c describing the observed $B - V$ colour in the supernova rest frame, as well as the corresponding covariance matrices which are essential for accurate evaluation of the likelihood.

In order to avoid possible biases related to selection effects of the surveys included in the supernova sample, we focus on relatively low-redshift supernovae for which these effects are minimised. Observational biases become non-negligible at high redshifts and the commonly used strategy to remove them is to simulate observations given a model of light curves and redshift-evolution of light curve parameters (see e.g. Scolnic et al. 2018). The current simulations involve the standard supernova calibration based on the Tripp calibration and as such they cannot be implemented in our modelling in a self-consistent way. Another complication arises from the fact that the prior weight w can be a function of redshift. Including this effect in the analysis of high-redshift data would require a full forward modelling of all components (cosmological model, Bayesian model of type Ia supernovae and survey selections) in order to control possible degeneracies. Conversely, considering low-redshift supernovae allows us to assume a constant weight w and to obtain constraints on supernova properties independently of cosmology and selection effects.

We select supernovae in the Hubble flow at redshifts between 0.023 and 0.15. We also apply additional selection criteria from Riess et al. (2016) regarding the allowed range of light curve parameters and the quality of light curve fits. Specifically, we include supernovae with the colour parameter $|c| < 0.3$ and the stretch parameter $|x_1| < 3$. These cuts eliminate a relatively small group of outliers for which the accuracy of interpolation built in the light curve SALT2 model is clearly worse than for normal type Ia supernovae. In addition, we omit supernovae with poor quality indicated by at least one of the following conditions: *fitprob* > 0.001 , error in the stretch parameter larger than 1.5, error in the peak time larger than 2 days or error in the corrected magnitude (approximated by the Tripp formula) larger than 0.2 mag.

This leaves us with 222 supernovae with high quality measurements of light curve parameters.

In order to test the impact of recent updates in the light curve fits, calibrations (Brout et al. 2022b) and redshift estimations (Carr et al. 2022), we repeat our analysis using supernova data from the *Pantheon+* catalogue (Brout et al. 2022a). We use 156 supernovae which overlap with our *SuperCal* sample. For supernovae with multiple light curve parameter measurements from different surveys (duplicates), we combine all independent results and compute single-measurement equivalents. Combining duplicates is necessary in order to avoid artificial weights which could otherwise bias the underlying distributions of light curve parameters. In these cases, the best-fit light curve parameters and covariance matrices are given by products of Gaussian probability distributions with the means and covariance matrices from the corresponding duplicates. In our analysis we omit bias corrections and systematic errors provided in the *Pantheon+* catalogue. The bias correction is primarily driven by the dust model of (Brout & Scolnic 2021) and thus it is not applicable to data modelling whose goal is to constrain extinction properties. Similarly, systematic errors are estimated for model-dependent derived distance moduli and therefore cannot be included in our analysis in a self-consistent way.

As an independent data set we also use the Foundation DR1 supernova sample (Foley et al. 2018; Jones et al. 2019). Compared to the *SuperCal* sample, this is a far more homogenous data set with all observations having been obtained with same instrument (Pan-STARRS) and a high accuracy of photometric calibration. The Foundation survey is a follow-up survey observing selected targets from other transient surveys. The targets are chosen as spectroscopically confirmed type Ia supernovae satisfying a number of secondary conditions. Therefore, one can expect that the resulting supernova sample is not fully unbiased and possible biases are related primarily to spectroscopic classification strategy. We omit several supernovae at redshift $z < 0.015$, for which the constraining power is significantly reduced due to large uncertainties related to peculiar velocities, so that the final sample contains 174 supernovae with a maximum redshift of 0.11. The Foundation DR1 catalogue provides best fit light curve parameters and covariance matrices based on the same light curve fitter as the *SuperCal* supernova sample (SALT2). The Foundation sample is used as a comparison data set in our study. Unless explicitly stated, all constraints and the final results are based on the *SuperCal* sample described above.

3.2 Baseline model

Fits to the supernova data unambiguously reveal the presence of two distinct supernova populations ($w = 0$ and $w = 1$ ruled with 4σ significance). It is also apparent that the main discriminator of the two populations is the stretch parameter x_1 . The two populations identified probabilistically in the data are supernovae with two decline rates of their light curves: fast declining with $\widehat{x}_1 \approx -1.3$ and slow declining with $\widehat{x}_1 \approx 0.4$. We will hereafter refer to these two populations respectively as population 1 (pop1) and population 2 (pop2) with the corresponding red (population 1) and blue (population 2) colour pallets in all figures.

The two populations appear to have quite different distributions of intrinsic colours and reddening. The observed supernova colours in population 1 are primarily driven by intrinsic colour and to a much lesser extent by dust reddening. This trend is reversed in population 2 supernovae whose observed colours are clearly driven by reddening due to dust. The relatively narrow ranges of reddening in population 1 and intrinsic colours in population 2 reduce the constraining power for $\{\widehat{R}_B, \sigma_{R_B}, \gamma\}$ in population 1 and β in population 2. These poorly constrained parameters are however consistent with their analogs from the opposite population and are well within the intervals given by their uncertainty. This shows that keeping $\{\widehat{R}_B, \sigma_{R_B}, \gamma, \beta\}$ independent in the two supernova populations cannot be constrained by the data. For this reason we will hereafter assume that these parameters are shared by both supernova populations, although both populations contribute unevenly to the final constraints. An analogous reduction in the parametrisation is justified in the case of the α parameter. Despite a striking difference between the distributions of x_1 in both populations, the linear relations between m_B and x_1 are consistent with having the same slopes in both populations. Assuming identically equal $\{\widehat{R}_B, \sigma_{R_B}, \gamma, \alpha, \beta\}$ parameters in both supernova populations defines the main class of models which we explore in more detail in our study.

The two left columns in Table 2 show constraints on all free parameters of our model with or without intrinsic scatter in both populations included as free parameters. Comparing these two cases we can see that including intrinsic scatter has virtually no impact on the remaining parameters. Furthermore, the best fit model is clearly consistent with vanishing intrinsic scatter in both populations. We find that the maximum likelihood σ_{int} is $\{0.03, 0.00\}$ and the corresponding 1σ upper limits are $\{0.06, 0.07\}$. The model with the intrinsic scatter is also strongly disfavoured with respect to its version with $\sigma_{\text{int}} \equiv 0$ in terms of the Bayesian Information Criteria yielding $\Delta BIC = +10.7$. This is the evidence that our two-population model provides a complete description of the supernova data on the Hubble diagram without invoking any extra scatter. In what follows, we shall consider its fully optimised version in which intrinsic scatter vanishes in both supernova populations. We will hereafter refer to this model as the baseline model.

Figure 2 and Table 2 show constraints on parameters obtained for the baseline model. As mentioned above, the primary difference between the two populations isolated by the model lies in their stretch parameter distributions. The two population have comparable ratios: 40 per cent for population 1 (fast declining supernovae) and 60 per cent for population 2 (slowly declining supernovae). Supernovae in population 2 appear to be intrinsically bluer than their analogs from population 1 and their intrinsic colours are less scattered around the distribution peak. These supernovae are also more affected by dust reddening and extinction. The distribution of apparent colours in this population results primarily from dust reddening and a typical $E(B-V)$ colour excess is 2 times larger than in population 1. We also find a tentative trend for population 1 supernovae being intrinsically brighter than their analogs from population 2 conditioned to have the same stretch parameter and intrinsic colour.

model	baseline		baseline+ σ_{int}		single population	baseline	
supernova sample	SuperCal 0.023 < z < 0.15		SuperCal 0.023 < z < 0.15		SuperCal 0.023 < z < 0.15	Foundation 0.015 < z < 0.11	
	SNe(pop1) fast declining	SNe(pop2) slowly declining	SNe(pop1) fast declining	SNe(pop2) slowly declining	pop1=pop2	SNe(pop1) fast declining	SNe(pop2) slowly declining
\widehat{M}_B	$-19.49^{+0.05}_{-0.05}$	$-19.40^{+0.07}_{-0.07}$	$-19.44^{+0.06}_{-0.07}$	$-19.37^{+0.07}_{-0.08}$	$-19.383^{+0.096}_{-0.092}$	$-19.44^{+0.09}_{-0.09}$	$-19.33^{+0.08}_{-0.08}$
\widehat{x}_1	$-1.31^{+0.28}_{-0.24}$	$0.41^{+0.14}_{-0.13}$	$-1.20^{+0.43}_{-0.35}$	$0.46^{+0.18}_{-0.16}$	$-0.250^{+0.075}_{-0.075}$	$-0.72^{+0.27}_{-0.27}$	$0.76^{+0.16}_{-0.13}$
σ_{x_1}	$0.70^{+0.16}_{-0.15}$	$0.64^{+0.09}_{-0.09}$	$0.76^{+0.23}_{-0.19}$	$0.59^{+0.12}_{-0.13}$	$1.093^{+0.055}_{-0.055}$	$0.88^{+0.15}_{-0.16}$	$0.52^{+0.10}_{-0.13}$
\widehat{c}_{int}	$-0.035^{+0.034}_{-0.033}$	$-0.112^{+0.033}_{-0.036}$	$-0.043^{+0.040}_{-0.042}$	$-0.103^{+0.034}_{-0.038}$	$-0.103^{+0.039}_{-0.042}$	$-0.114^{+0.037}_{-0.037}$	$-0.133^{+0.031}_{-0.031}$
$\sigma_{c_{\text{int}}}$	$0.077^{+0.011}_{-0.011}$	$0.042^{+0.013}_{-0.013}$	$0.069^{+0.017}_{-0.019}$	$0.043^{+0.014}_{-0.015}$	$0.047^{+0.016}_{-0.016}$	$0.056^{+0.022}_{-0.021}$	$0.034^{+0.021}_{-0.022}$
τ	$0.017^{+0.008}_{-0.009}$	$0.034^{+0.008}_{-0.008}$	$0.023^{+0.015}_{-0.015}$	$0.037^{+0.011}_{-0.010}$	$0.035^{+0.008}_{-0.010}$	$0.041^{+0.012}_{-0.015}$	$0.034^{+0.012}_{-0.014}$
α	$0.185^{+0.024}_{-0.025}$		$0.171^{+0.025}_{-0.024}$		$0.139^{+0.009}_{-0.008}$		$0.153^{+0.036}_{-0.036}$
β	$3.089^{+0.243}_{-0.238}$		$3.174^{+0.275}_{-0.334}$		$3.193^{+0.532}_{-0.478}$		$3.116^{+0.251}_{-0.251}$
\widehat{R}_B	$4.132^{+0.647}_{-0.591}$		$3.964^{+0.725}_{-0.669}$		$3.698^{+0.515}_{-0.497}$		$3.789^{+0.551}_{-0.546}$
σ_{R_B}	$0.946^{+0.313}_{-0.283}$		$0.781^{+0.371}_{-0.350}$		$0.751^{+0.343}_{-0.302}$		$0.843^{+0.298}_{-0.265}$
γ	$3.231^{+1.236}_{-1.258}$		$2.717^{+1.321}_{-1.276}$		$3.129^{+1.293}_{-1.360}$		$3.296^{+1.197}_{-1.234}$
w	$0.397^{+0.109}_{-0.097}$		$0.453^{+0.182}_{-0.148}$		$\equiv 0$		$0.594^{+0.123}_{-0.117}$
σ_{int}	$\equiv 0$	$\equiv 0$	< 0.055	< 0.073	$0.054^{+0.025}_{-0.028}$	$\equiv 0$	$\equiv 0$
$\langle E(B - V) \rangle$	$0.052^{+0.029}_{-0.030}$	$0.102^{+0.036}_{-0.033}$	$0.058^{+0.039}_{-0.037}$	$0.093^{+0.037}_{-0.034}$	$0.103^{+0.042}_{-0.039}$	$0.120^{+0.036}_{-0.036}$	$0.101^{+0.035}_{-0.035}$
ΔBIC	0		+10.8		+6.4	-	

Table 2. Best fit hyperparameters of prior probability distributions describing latent variables in two distinct supernova populations (see Table 1 for the notation). The constraints were obtained for the baseline model (“baseline”), its extension including intrinsic scatter in both supernovae populations as extra free parameters (“baseline+ σ_{int} ”) and the baseline model assuming a single population (“single population”). The table shows the results from fitting all three models to *SuperCal* supernova sample and independently the baseline model to the Foundation DR1 sample (“Foundation”). Best fit results are provided as the posterior mean values and errors of the credibility range containing 68 per cent of the marginalised probabilities (except for σ_{int} in the “baseline+ σ_{int} ” model where we show 68 per cent upper limits). Hyperparameters which are not shared by the supernova population are shown in designated columns of each model. Shared parameters, e.g. $\{\alpha, \beta, \widehat{R}_B, \sigma_{R_B}, \gamma\}$ in the baseline mode, are shown once between the columns corresponding to the supernova populations. The two bottom lines show the mean colour excess $\langle E(B - V) \rangle$ derived from the Markov chains and the Bayesian Information Criterion $BIC = k \ln(N) - 2 \ln L_{\text{max}}$, where N is the number of supernovae, k is the number of model parameters and L_{max} is the maximum likelihood.

3.3 Prior distribution of $E(B - V)$

A very important finding of our analysis is a clear preference for a peaked (two-tailed) distribution of $E(B - V)$ colour excess ($\gamma > 1$) over the exponential distribution ($\gamma = 1$). This property has a direct impact on implied supernovae intrinsic colours. As shown in Figure 2, supernovae in both populations are intrinsically bluer (more negative \widehat{c}_{int}) than in models assuming an exponential distribution of $E(B - V)$. We find evidence for a two-tailed distribution of $E(B - V)$ in analysis of both supernova samples (*SuperCal* and Foundation DR1). The property is not related to two-population

assumption and it holds for reduced models assuming a single supernova population (see Table 2).

3.4 Comparison of two supernova samples

It is instructive to compare the properties of the baseline model inferred from the *SuperCal* supernova sample to those from the Foundation DR1 sample. Initial fits with the Foundation data are affected by insufficient constraining power for β with a nearly flat marginalized posterior distribution. This most likely results from slightly larger errors on the

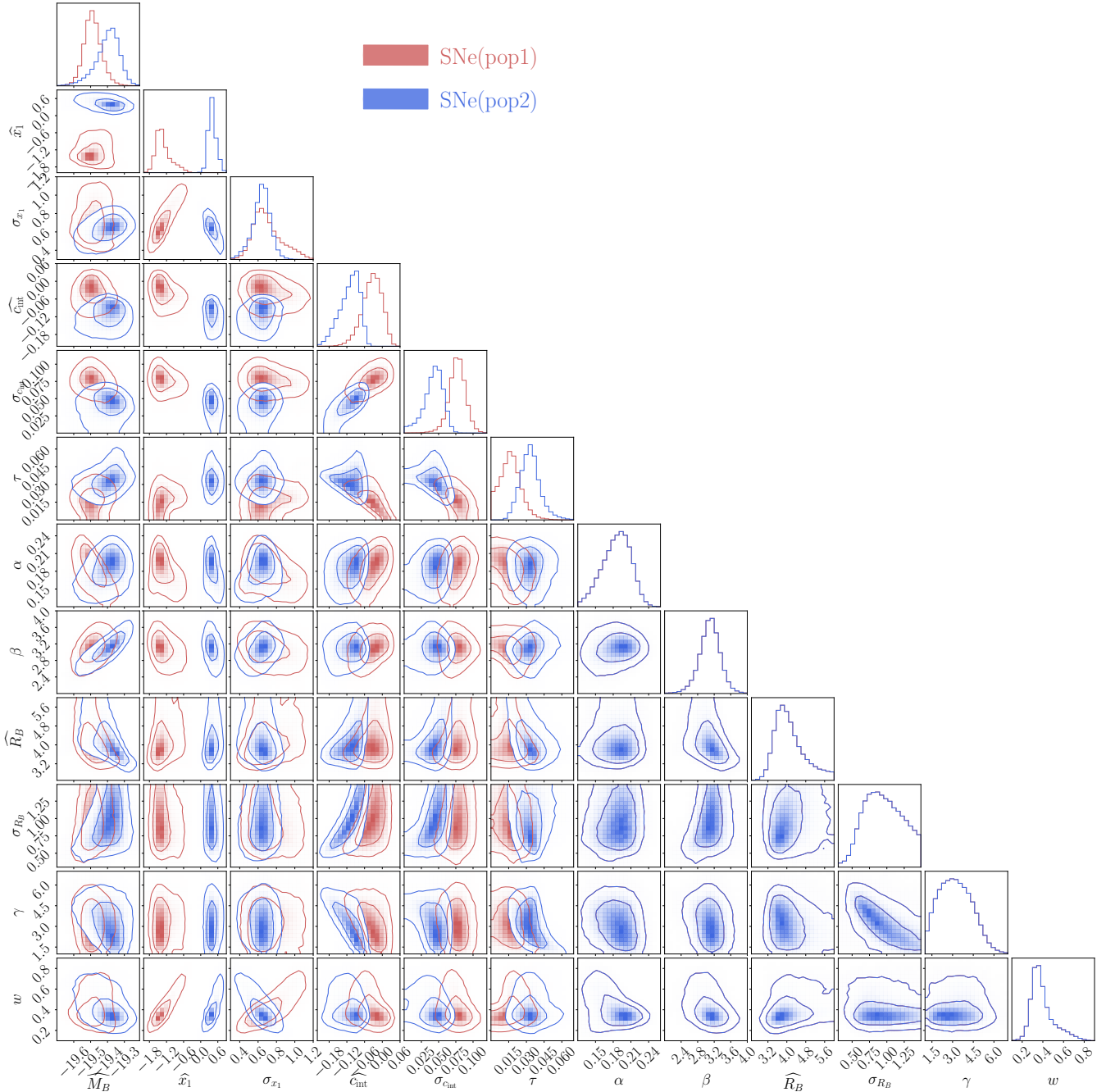


Figure 2. Constraints on hyperparameters of the baseline model obtained for the *SuperCal* supernova sample. The red and blue contours show constraints on parameters in the two supernova populations: population 1 (fast declining supernovae, red) and population 2 (slowly declining supernovae, blue). For the sake of better readability, the corner plot is compressed by overlaying the panels with the corresponding sets of hyperparameters. The contours show 1σ and 2σ confidence regions containing 68 and 95 per cent of 2-dimensional marginalised probability distributions.

colour parameters c (20 per cent larger than in the *SuperCal* supernova sample) and from the fact that the Foundation data favour narrower distributions of intrinsic colours in both supernova populations for which measuring the slope β becomes less precise. We circumvent this problem by adopting constraints on β from the *SuperCal* sample as a prior probability in the analysis of the Foundation data. Comparing the results obtained from the two supernova samples (see Table 2) it is apparent that virtually all properties of

the baseline model are quite similar. In particular, the same peaked shape of the distribution in $E(B - V)$ with $\gamma \approx 3.9$ is favoured over the exponential model by both supernova sample. Both data sets place fully consistent constraints on the distribution of R_B with $\widehat{R}_B \approx 4$ and $\sigma_{R_B} \approx 0.9$. The difference between the two supernova populations in terms of dust reddening and intrinsic colours found for the *SuperCal* sample are less pronounced in the Foundation sample. This is partially caused by a weaker constraining power of

the Foundation data resulting in larger errors of hyperparameters related to the observed supernova colour, e.g. $\sigma_{c_{\text{int}}}$ and τ . The Foundation sample seems to favour a slightly elevated fraction of population 1 supernovae, although the difference is not statistically significant (1.3σ).

The Foundation sample appears to have less colour-dependent scatter than the *SuperCal* sample. When refitting the baseline model with free intrinsic scatter in both supernova populations, we find an upper limit for scatter in the extinction parameter, i.e. $\sigma_{R_B} < 0.34$, and a clear preference for achromatic scatter with $\sigma_{\text{int}} = 0.1 \pm 0.02$. Therefore, the scatter σ_{R_B} obtained for the Foundation sample and shown in Table 2 is to some extent driven by the assumption that intrinsic scatter vanishes in the baseline model.

3.5 Robustness tests

Repeating our fits using supernovae with the most recent updates of light curve parameters and redshifts from the *Pantheon+* compilation, we find a broad agreement with the results obtained for the *SuperCal* sample. In Appendix B we show constraints on parameters of the baseline model with the mean extinction parameter $\widehat{R_B}$ allowed to be independent in the two supernova populations. The properties of the best fit model resemble closely those obtained for the *SuperCal* and most parameters derived from the two data sets remain well within their errors. The only noticeable difference is a stronger degeneracy between intrinsic colour, reddening and $\widehat{R_B}$ in population 1 (see Fig. B1).

In order to test a potential impact of survey limiting magnitudes on our results, we repeat our analysis including redshift-dependent bias estimated for low- z surveys in Scolnic et al. (2018). Considering two models explored in Scolnic et al. (2018), we find that the bias has a negligible impact with relative shifts of the best fit values not exceeding 20 per cent of the uncertainties. Furthermore, we also checked that restricting our analysis to nearby supernovae at $z < 0.08$, which effectively mitigates potential observational biases in a model independent way, returns best fit parameters well within the errors of the best fit model based on the whole sample.

3.6 Hubble residuals

The baseline model provides a complete probabilistic description of type Ia supernova as standardisable candles. The unavoidable intrinsic scatter on supernova Hubble diagrams constructed by applying the standard Tripp formula (or its extensions, such as including additional corrections related to the host stellar mass) is fully accounted for in terms of dust extinction and differences between intrinsic and extrinsic properties of two supernova populations. In order to appreciate the explanatory potential of our model, we compute the distribution of supernovae in the space of light curve observables $\{m_B - \mu, x_1, c\}$ predicted by the baseline model and compare to the actual distribution of supernovae from the observational sample. We calculate the predicted distribution in a Monte Carlo way by sampling from the prior distributions of all latent variables and generating marginalised distributions in the observable space based on eq. (3). We use best fit parameters of the baseline model ($\sigma_{\text{int}} \equiv 0$) mea-

sured from the *SuperCal* supernova sample. We subtract the effect of distances by considering $m_B - \mu$ instead of m_B .

It is instructive to express supernova magnitude m_B relative to a model given the Tripp formula (Tripp 1998), i.e.

$$m_{B \text{ Tripp}} = M_{B \text{ T}} + \mu(z) - \alpha_{\text{T}} x_1 + \beta_{\text{T}} c. \quad (8)$$

This conversion reduces to a change of one variable in the model's predictions, but for the actual supernova data it generates genuine residuals expected on the corresponding Hubble diagram. For the sake of complete consistency with the data we use $\{M_{B \text{ T}}, \alpha_{\text{T}}, \beta_{\text{T}}\}$ measured directly from the supernova sample. Performing a fit based on the likelihood given by

$$\ln L \propto -\frac{1}{2} \sum_i^N \frac{[m_{B i} - m_{B \text{ Tripp}}(z_i, c_i, x_{1 i})]^2}{\sigma_{\text{tot } i}^2 + \sigma_{\text{int } \text{T}}^2} \quad (9)$$

$$-\frac{1}{2} \sum_i^N \ln(\sigma_{\text{tot } i}^2 + \sigma_{\text{int } \text{T}}^2) \quad (10)$$

where $\sigma_{\text{tot } i}$ is the total uncertainty including contributions from all elements of the covariance matrix and uncertainty related to peculiar velocities (see e.g. Brout & Scolnic 2021; Wojtak & Hjorth 2022), and $\sigma_{\text{int } \text{T}}$ is an extra free parameter describing intrinsic scatter, we obtain $M_{B \text{ T}} = -19.338 \pm 0.009$, $\alpha_{\text{T}} = 0.128 \pm 0.008$, $\beta_{\text{T}} = 3.00 \pm 0.12$ and $\sigma_{\text{int } \text{T}} = 0.11 \pm 0.008$ (assuming consistently the same cosmological model with $H_0 = 70 \text{ km s}^{-1} \text{ Mpc}^{-1}$ as in the main analysis).

Figure 3 compares the distribution of residuals in Tripp formula supernova magnitudes on the Hubble diagrams relative to the baseline model's predictions, as a function of stretch parameter x_1 or colour parameter c . The panels demonstrate how precisely the model captures all subtle features in the distribution of the Hubble residuals and supernova light curve parameters. In particular, the model reproduces the conspicuous bimodality in the stretch parameter and a clear trend of Hubble residuals increasing with the colour parameter. The latter is primarily a manifestation of a rather large scatter in R_B , i.e. $\sigma_{R_B} \approx 0.9$, giving a characteristic pattern of divergent isodensity contours towards positive colour parameters ($c > 0$) in population 2 supernovae (whose observed colours are dominated by dust reddening). Here we can also see excess of positive Hubble residuals at $0 \lesssim c \lesssim 0.2$ (about 2 times more supernovae with residuals $(m_B - m_{B \text{ Tripp}}) > 0.2$ than those with $(m_B - m_{B \text{ Tripp}}) < -0.2$) which can be ascribed to the fact that the bulk of R_B values allowed by the model (including $\widehat{R_B}$) are larger than the colour correction coefficient β_{T} of the Tripp calibration. Both the apparent asymmetry and colour-dependent scatter in the Hubble residuals have been described in several studies (see e.g. Brout & Scolnic 2021; Popovic et al. 2021). These are anomalous features in the standard framework based on the Tripp calibration. They play a key role in disentangling the effects of intrinsic colours from dust reddening in both supernova populations.

Comparing Hubble residuals in supernova populations from our modelling and analogous populations of young and old supernovae from Rigault et al. (2020), we find a similar scatter in population 2 (0.13) as in the corresponding young supernovae, but two times smaller scatter in population 1 than in the corresponding old supernovae. To a large extent

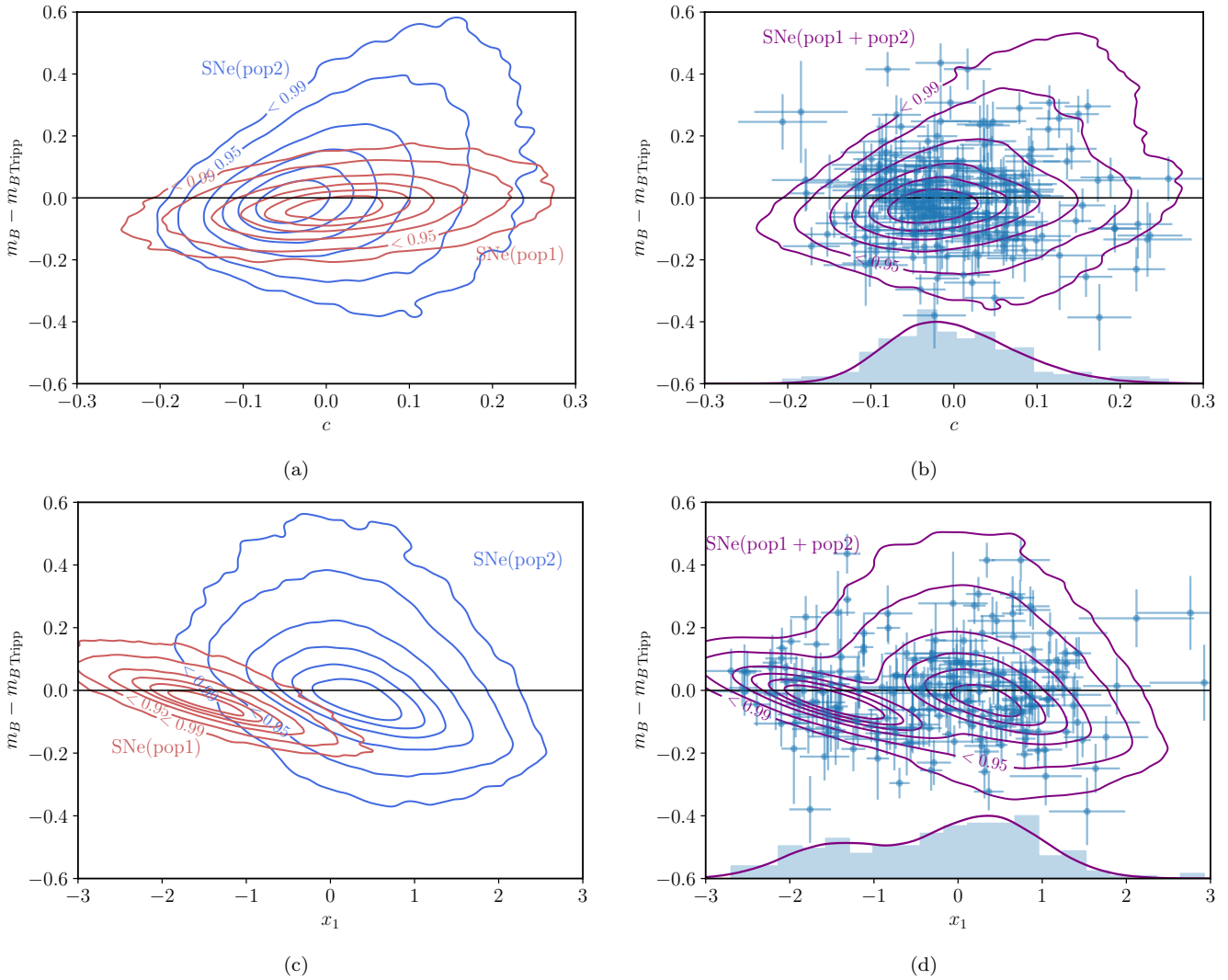


Figure 3. Distributions of the Hubble residuals in type Ia supernova peak magnitudes (standardised using baseline model relative to Tripp calibration), as a function of colour parameter c or stretch parameter x_1 . The symbols show supernova data from the *SuperCal* supernova sample used in this study, while contours show the distributions implied by the best fit baseline model. The left panels illustrate the effect of differences between the distributions of latent variables in the two supernova populations (population 1 – fast declining; population 2 – slow declining) on the observed light curve parameters. The right panels demonstrate that the best fit baseline model provides a complete and accurate description of the apparent Hubble residuals including (i) bimodality in the distribution of x_1 , (ii) asymmetries between positive and negative residuals and (iii) scatter in the Hubble residuals increasing with the supernova colour parameter. The histograms show the distributions of observed supernova light curve parameters. They are compared to the best fit model shown with the corresponding solid lines. All apparent features in the distribution of the Hubble residuals and observed supernova colours are accounted for in terms of extinction properties and differences between intrinsic (intrinsic colour) and extrinsic (dust reddening) properties of the two model populations.

the apparent difference results from the fact that the old population of Rigault et al. (2020) does not consist solely of fast decliners, but mixes high- and low-stretch supernovae.

4 DISCUSSION

The baseline model developed in this study is the first Bayesian hierarchical model of type Ia supernovae which provides a complete explanation of Hubble residuals in terms of intrinsic properties of type Ia supernovae and extrinsic effects of dust. The key new element is the theoretically and observationally motivated premise that type Ia supernovae

originate from two distinct populations most likely associated with star-forming and passive environments. The model recovers several important findings obtained with previous Bayesian analyses assuming a single supernova population, but it also refines many details which are relevant to building a consistent holistic picture of type Ia supernovae and their environments. In the following, we describe the physical properties implied by our model and put them in a broader context of type Ia supernova studies.

4.1 Two populations

A two-population model is strongly favoured by the supernova data. Fitting its analog with a single population we find that the model can account for only a fraction of the intrinsic scatter in the Hubble residuals (see Table 2). In a single-population model, a physically motivated dust model with a wide range of R_B values reduces the intrinsic scatter from $\sigma_{\text{int}} \approx 0.11$ for the Tripp calibration to $\sigma_{\text{int}} \approx 0.06$. This effect is also found in several independent studies employing similar single-population Bayesian hierarchical models (Mandel et al. 2017; Thorp et al. 2021; Mandel et al. 2022). Further reduction of the intrinsic scatter, however, can only be achieved by considering two supernova populations. In term of the Bayesian Information Criterion, we find the the baseline model is strongly favoured by the *SuperCal* supernova sample over its single-population analog with $\Delta BIC = -6.8$.

The two supernova populations emerging from our baseline model can be tentatively interpreted as supernovae originating from an old (delayed) progenitor channel (population 1) and a young (prompt) progenitor channel (population 2). Assuming that there exists a rather unambiguous mapping between the model populations and these progenitor channels, we expect that the weight parameter $(1 - w)$ in our model can be regarded as an estimate of the fraction of supernovae from the prompt progenitor channel. The most rigorous measurement of the population fraction was obtained from fitting redshift dependence of type Ia supernova volumetric rate (Rodney et al. 2014). The key idea of this measurement is that the observed volumetric rate can be probabilistically split into two distinct components associated with the prompt progenitor channels (following the star formation history) and the delayed progenitor channel (lagged behind the star formation history with a characteristic time delay distribution $\propto t^{-1}$ expected for double-degenerate binary systems) (Maoz et al. 2014). Analysis of type Ia supernova volumetric rate measurements as a function of redshift showed that the global fraction of prompt type Ia supernovae is $f_p = 0.53^{+0.14}_{-0.36}$ (Rodney et al. 2014). Taking into account the star formation history and the time delay distribution assumed in Rodney et al. (2014), this implies that the prompt channel fraction at redshift $z = 0$ is $f_p(z = 0) = 0.30^{+0.08}_{-0.20}$. Independent estimates of f_p can be derived from observations of blueshifted Na I D absorption features in supernova spectra. These absorption features are interpreted as a signature of circumstellar material from a non-degenerate companion star of supernova progenitor and thus they can be used to differentiate between single and double degenerate progenitor channels (or related delayed and prompt channels). Observations yield $f_p(z = 0)$ ranging between 0.2 (Maguire et al. 2013) to 0.5 (Phillips et al. 2013). The corresponding fractions measured in our analysis, i.e. $1 - w = 0.60 \pm 0.1$ from the main and $1 - w = 0.41 \pm 0.12$ from the Foundation DR1 sample, appear to be consistent with the upper limit of the above-mentioned estimates. Andersen & Hjorth (2018) modelled the SN Ia rate as a function of specific star formation rate of their host galaxies and found $f_p(z = 0) = 0.10^{+0.10}_{-0.06}$.

Population 2 (slowly declining) supernovae appear to be on average intrinsically bluer than population 1, with $\Delta c_{\text{int}} = -0.077 \pm 0.032$. Their mean intrinsic colour is

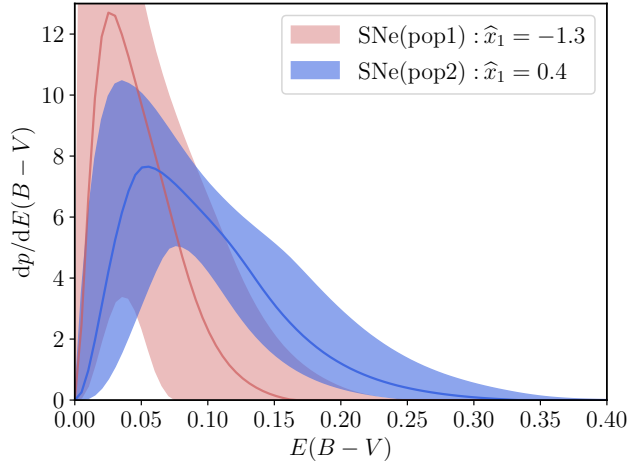


Figure 4. Distribution of colour excess $E(B - V)$ in the two supernova populations emerging from the baseline model fitted to the *SuperCal* supernova sample. The lines and contours show the best fit model predictions and the corresponding 68 per cent uncertainties computed by sampling from the corresponding MCMC. Both populations are described by peaked distributions with a maximum at $E(B - V) > 0$. The scale of reddening in population 2 (slowly declining) supernovae is ~ 2 times larger than in population 1 (fast declining supernovae).

$\Delta c_{\text{int}} \approx -0.03$ bluer than the previous estimates from analyses assuming single supernova population (Popovic et al. 2021; Brout & Scolnic 2021). Slowly declining supernovae (population 2) also seem to be 0.09 ± 0.07 mag fainter. This is only an indicative offset, but it is consistently found in both supernova samples. We note that a similar trend was found for the populations of fast and slowly declining supernovae selected by the stellar age supernova environments (Rigault et al. 2013, 2020; Maoz et al. 2014).

4.2 Dust

Supernovae from the two populations discerned by the baseline model exhibit different degrees of dust reddening as measured by the scale parameter τ . Based on the model's parameters we conclude that population 1 (fast declining) supernovae are associated with dust-poorer environments with the mean colour excess $\langle E(B - V) \rangle \approx 0.052 \pm 0.030$, while population 2 (slowly declining) supernovae with dust-rich environments with $\langle E(B - V) \rangle \approx 0.102 \pm 0.035$. This difference is not surprising given a wide range of observations showing that type Ia supernovae similar to those in population 2 (slowly declining light curves) are typically found in highly star-forming and thus dust rich environments (see e.g. Rigault et al. 2020). It is clearly supported by the data of the *SuperCal* supernova sample for which we find a significance level of 2.3σ (higher than expected from a summary statistics shown in Table 2 due to a strong correlation between τ parameters in the two populations). It is not apparent in the Foundation sample, most likely due to a weaker constraining power of the Foundation data.

Dust extinction inferred from both supernova samples is described by a wide range of extinction coefficients. The mean value of R_B , i.e. $\widehat{R}_B \approx 4.1$, is fully consistent with an average extinction measured directly in the Milky Way

(Fitzpatrick 1999; Schlafly et al. 2016) and nearby galaxies (Draine 2003). The range of extinction coefficients in individual sight lines allowed by the scatter $\sigma_{R_B} = 0.9$ overlaps largely with a range $3 \lesssim R_B \lesssim 7$ measured in the Milky Way (Fitzpatrick & Massa 2007; Draine 2003). We also note that the recently found anomalously high colour correction of type Ia supernovae in host galaxies with observed Cepheids ($\beta_T = 4.6 \pm 0.4$; Wojtak & Hjorth 2022) is consistent with a typical extinction coefficient found in our analysis. We interpret this coincidence as an indication that supernovae in the calibration sample of the SH0ES program originate primarily from population 2 (supernovae with colours driven predominantly by dust reddening). In the recent SH0ES measurement of the Hubble constant, the adopted approach to mitigating differences between supernovae in Cepheid host galaxies and the Hubble flow relies on selecting supernovae in late-type galaxies similar to those in the calibration sample (Riess et al. 2022).

Dust extinction is primarily constrained by population 2 supernovae whose observed colours are dominated by dust reddening. Constraining $\widehat{R_B}$ independently in population 1 by fitting a one-parameter extension to the baseline model to the *SuperCal* supernova sample yields $\widehat{R_B} = 3.6_{-1.2}^{+1.3}$ and shows no indication of any difference between extinction properties in the two supernova populations. Our constraints on the distribution of R_B are also broadly consistent with the previous estimates based on Bayesian hierarchical models with a single supernova population (see e.g. Thorp et al. 2021) and alternative estimates based on modelling supernova colours in multi-band observations, for a similar range of reddening with $E(B - V) \lesssim 0.3$ (Burns et al. 2014). As demonstrated in Table 2, alternating between single- and two-population models has a rather negligible impact on the estimation of the mean and scatter of the extinction coefficient R_B .

Constraints on the shape parameter γ demonstrate that the supernova data favour a peaked (two-tailed) distribution of colour excess $E(B - V)$, well represented by a gamma distribution with $\gamma \approx 3.3$, over the commonly assumed exponential model (Thorp et al. 2021; Mandel et al. 2017; Brout & Scolnic 2021). The shape of the distribution as well as the difference between the two supernova populations in terms of the mean colour excess are illustrated by Fig. 4. The distributions shown in the figure were computed for the baseline model fitted to the *SuperCal* supernova sample. Compared to its exponential analog, peaked distributions of colour excess $E(B - V)$ enhance the effect of dust reddening in the observed supernova colours resulting in intrinsically bluer implied intrinsic colours. This property is shown in Figure 2 as a correlation between $\widehat{c_{\text{int}}}$ and γ .

The role of supernova populations in explaining the Hubble residuals in terms of extinction properties was realised to some extent by Brout & Scolnic (2021). They showed that deriving R_B distributions in two separate bins of supernova host stellar masses gives a more complete description of the Hubble residuals. Their analysis based on a single-population model for intrinsic supernova properties implies that high stellar mass ($> 10^{10} M_\odot$) host galaxies exhibit substantially lower extinction coefficients with $\widehat{R_B} \approx 2.5$ compared to $\widehat{R_B} \approx 3.8$ for low-mass hosts ($< 10^{10} M_\odot$). It is not obvious, however, which physical processes can effectively fine tune dust properties in a way that they can match

the apparent difference in R_B between high and low stellar mass host galaxies and explain the corresponding transition scale in the stellar mass. In contrast, our two-population model implies dust properties which can be fairly easily reconciled with existing observations without any necessary fine tuning or need for non-standard dust properties. While extinction properties in all supernova host galaxies resemble closely those known from the Milky Way, the two supernova populations are characterised by different average column densities of dust which can be naturally associated with the observed differences between star formation rates of their local environments.

4.3 Host galaxy properties

Our model enables us to assign a probability of belonging to one of the two populations to each supernova. This classification can be performed by computing relative probabilities of finding a supernova with a given set of light curve parameters and originating from either of the two populations. The relative probabilities are given by the prior probabilities of the two supernova populations marginalised over latent variables, subject to a set of measured light curve parameters $\boldsymbol{\xi}_{\text{obs i}}$. This leads to the following probability ratio

$$\frac{p(\text{SN}_{\text{pop 1}})}{p(\text{SN}_{\text{pop 2}})} = \frac{w \int \mathcal{G}[\boldsymbol{\xi}(\boldsymbol{\phi}); \boldsymbol{\xi}_{\text{obs i}}, \mathbf{C}_{\text{obs i}}] p_{\text{prior 1}}(\boldsymbol{\phi}) d\boldsymbol{\phi}}{(1-w) \int \mathcal{G}[\boldsymbol{\xi}(\boldsymbol{\phi}); \boldsymbol{\xi}_{\text{obs i}}, \mathbf{C}_{\text{obs i}}] p_{\text{prior 2}}(\boldsymbol{\phi}) d\boldsymbol{\phi}} \quad (11)$$

which we use as a continuous variable to probabilistically classify supernovae to the model populations. We estimate the most likely range of the probability ratios by propagating the values of hyperparameters from the precomputed Markov chains to eq. (11). The final estimates are then computed as the mean and scatter of the logarithmic probability ratios.

Figure 5 shows the probabilistic classification of supernovae from the *SuperCal* supernova sample into the two populations of the baseline model, as a function of the morphological type or stellar mass of the host galaxy. The classification is based on the baseline model fitted to the *SuperCal* supernova sample. The stellar mass estimates were obtained from modelling multi-band photometric observations of the host galaxies and they are taken from the corresponding supernova catalogue (Scolnic et al. 2015). The morphological type is quantified by a continuous morphological variable T introduced by de Vaucouleurs (1974) and provided by the HyperLeda database¹. This metric is estimated by combining a wide range of various indicators of galaxy morphology, e.g. photometric structure, colour index, or hydrogen content. Its values can be mapped directly into the Hubble sequence with $T = -5$ for the earliest types (E) and $T = 10$ for the latest types (irregular galaxies), as indicated in Figure 5.

Figure 5 demonstrates that the relative fractions of the supernova populations determined in our model vary across morphological types and stellar masses of the host galaxies. It is apparent that early type galaxies with $T < -1$ are primarily dominated by population 1 (fast declining) supernovae, while late type galaxies host both populations. This

¹ <http://leda.univ-lyon1.fr>

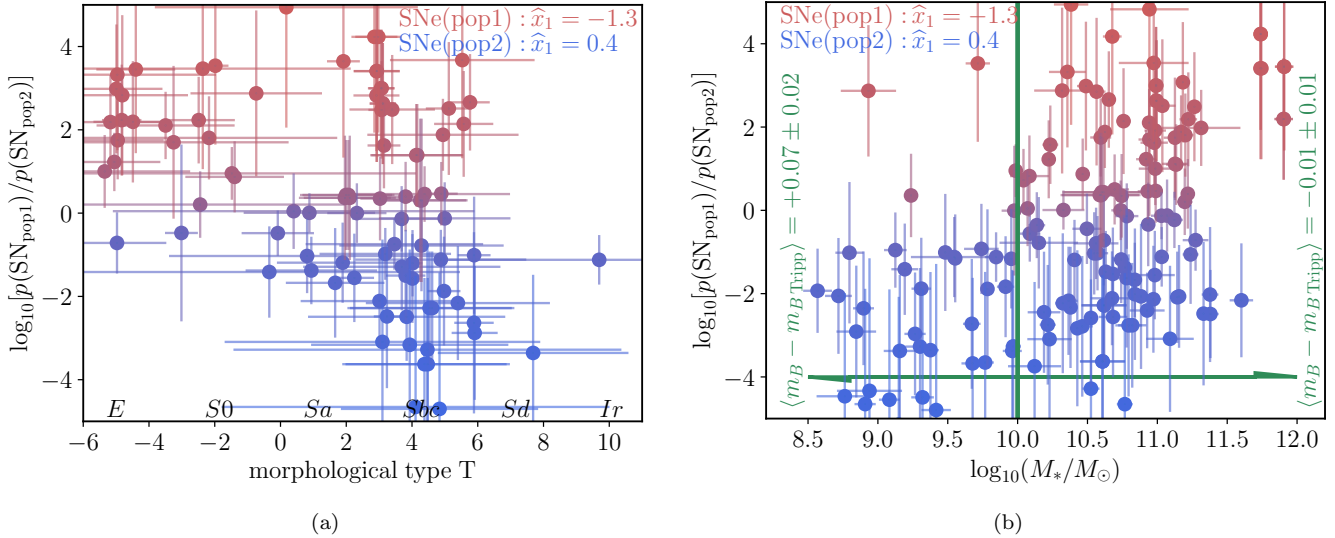


Figure 5. Populations of individual supernovae as a function of morphological type or stellar mass of the host galaxy. The populations are assigned in a probabilistic way by comparing probabilities of a given supernova originating from either of the two populations in the baseline model. The assigned populations are shown both on vertical axes of the plots and as color coding of the data points. The panels show that population 2 (slowly declining) supernovae do not occur in early type galaxies, while population 1 (fast declining) supernovae are typically not found in galaxies with stellar masses below $\sim 10^{10}M_\odot$. Both properties can be explained by assuming that population 1 (2) supernovae are associated with old (young) stellar populations and by accounting for how the ratio of young-to-old stellar populations changes across morphological types and stellar masses. The right panel also shows that the commonly used mass step correction in type Ia supernova standardisation can be attributed to an effect of breaking the symmetry between the two supernova populations (and the associated stellar populations) below $\sim 10^{10}M_\odot$.

corroborates earlier studies which showed that low star formation (old stellar population) environments are predominantly populated by fast declining (low-stretch) supernovae (Rigault et al. 2013, 2020; Pruzhinskaya et al. 2020). The same relation between the supernova populations and the underlying stellar populations can be used to explain the apparent dependency of supernova populations on the stellar mass of the host galaxy. Studies of galaxy properties from the Sloan Digital Sky Survey showed that galaxies with stellar masses below $\sim 10^{10}M_\odot$ are strongly dominated by young stellar populations, while their analogs above this mass limit mix young and old stellar populations (Kauffmann et al. 2003). Consequently, low-mass galaxies with stellar masses below $\sim 10^{10}M_\odot$ are expected to host predominantly population 2 (slowly declining) supernovae, while high-mass galaxies are expected to produce supernovae from both populations.

The dependency on the host stellar mass shown in Figure 5 is closely related to the commonly used mass step correction in the standardisation of type Ia supernovae (see e.g. Kelly et al. 2010; Scolnic et al. 2018; Smith et al. 2020). The correction is intended to reduce intrinsic scatter in the supernova Hubble diagrams by subtracting the empirically measured difference between Hubble residuals of supernovae in galaxies with stellar masses above or below $\sim 10^{10}M_\odot$, where the magnitude difference is typically found in range (0.04 – 0.08) mag (0.08 ± 0.02 for the *SuperCal* supernova sample used in our study). As clearly demonstrated in Figure 5, the transition mass of the mass step correction (see the green line) coincides with the abrupt change of relative fractions of the two supernova populations. This suggests that the empirical mass correction is not a fundamental rela-

tion between supernovae and the host galaxies, but rather an emerging property resulting from (i) the presence of two distinct supernova populations associated with old and young stellar populations and (ii) a step-like change of the stellar population ratio at stellar mass $\sim 10^{10}M_\odot$.

In order to test whether a mass step correction is needed in our model, we compute supernova Hubble residuals with model peak magnitudes given by eq. (1). We use mean intrinsic colour and reddening $E(B - V)$ derived from sampling the underlying prior distribution conditioned to the measured colour parameters of each supernova. Predicted peak magnitudes of each supernova are then calculated using population types shown in Figure 5. Assuming that R_B is given by the same best fit mean value across all host masses, we find that our model decreases the mass step by 30 per cent from 0.08 to 0.055. Further reduction of the mass step requires introducing a mass-dependent \widehat{R}_B . In fact, only 12 percent relative difference between \widehat{R}_B in the high- and low-mass supernova hosts ($\widehat{R}_B \approx 4.4$ for high-mass hosts and $\widehat{R}_B = 3.9$ for low-mass hosts) allows to eliminate the difference between mean Hubble residuals in the two mass bins. Thus, in our modelling based solely on supernova data, the required difference is accounted for by a fraction of the measured scatter in R_B (30 per cent of σ_{R_B}). This finding is qualitatively consistent with Brout & Scolnic (2021) who showed that the mass step is primarily driven by Hubble residuals of red supernovae and thus it can be attributed to a difference between extinction coefficients in the host stellar mass bins (higher extinction in low-mass hosts; see also Wiseman et al. 2022). However, the effect is much more subtle in our case and \widehat{R}_B values in both mass bins are compatible with a range

of typical extinction coefficients measured in the Milky Way (Fitzpatrick & Massa 2007; Legnardi et al. 2023).

5 SUMMARY AND CONCLUSIONS

We have presented a novel Bayesian hierarchical model for constraining the distributions of intrinsic properties of type Ia supernovae and dust properties in their sight lines from supernova light curve parameters. The model incorporates the observationally motivated assumption that there are two distinct supernova populations and a physically motivated *ansatz* for the prior distribution of dust reddening. We have fitted the model to SALT2 light curve parameters of type Ia supernovae in the Hubble flow. The main properties of the best fit model and the resulting supernova populations can be summarised as follows:

(1) The model is strongly favoured over its alternative assuming only one supernova population (with $\Delta BIC = -6.4$).

(2) The model discerns two overlapping supernova populations distinguished primarily by the mean stretch parameter: supernovae with low stretch (fast declining light curves) and high stretch (slowly declining light curves).

(3) Supernovae from the identified population of slow decliners (high stretch) appear to be intrinsically bluer (on average $\Delta c_{\text{int}} = -0.077 \pm 0.029$), with two times stronger dust reddening in their sight lines than supernovae from the opposite population.

(4) Extinction in both supernova populations is described by a broad distribution of R_B with maximum ($R_B \approx 4.1$) coinciding with the average extinction measured in the Milky Way, and dispersion $\sigma_{R_B} \approx 0.9$.

(5) The distribution of dust reddening inferred from the supernova data has a distinct maximum and two tails, in contrast to the exponential model commonly employed in the previous studies.

(6) Intrinsic scatter in the supernova Hubble diagrams vanishes and the model provides a complete explanation of the Hubble residuals arising from the commonly used Tripp calibration (Tripp 1998).

The model presented in our work is entirely driven by supernova data. The two populations identified by the model are found to be associated with old and young (star forming) stellar populations and thus they closely coincide with analogous supernova populations identified in previous studies using host galaxy information. The young stellar environment appears to be a natural source of higher column densities of dust (reddening) measured in population 2. The apparent correspondence between the supernova populations and underlying stellar environments provides also a simple framework for understanding the origin of the well known stellar mass step correction in the Tripp calibration. The correction results to some extent from a partial separation of supernova populations driven by an abrupt change of mixing the underlying stellar populations at stellar mass $10^{10} M_{\odot}$.

The proposed model can be effectively used to standardise type Ia supernovae for cosmological analyses. In this approach, one can fit a cosmological model simultaneously with the physical properties of type Ia supernovae and extinction in their sight lines. This is the only complete strategy which allows for modelling the expected redshift evolution of

the supernova population fractions (in relation to the star formation history) and perhaps cosmic dust, which otherwise could potentially bias cosmological parameters (Rigault et al. 2020). The model will also be indispensable for providing a quantitative and physical explanation of the recently reported anomalously high slope of the apparent colour correction of type Ia supernovae in the calibration sample from the local measurement of the Hubble constant (Wojtak & Hjorth 2022). The measured colour correction is consistent with being entirely due to extinction with Milky Way-like dust properties. This suggests that the calibration sample contains supernovae originating primarily from only one of the two populations, in contrast to the Hubble flow which visibly mixes the two populations. Quantitative analysis of this problem using the model developed in this study and its possible implications for understanding hidden systematic errors or biases in the local measurements of the Hubble constant will be the subject of our forthcoming paper.

ACKNOWLEDGMENTS

This work was supported by a VILLUM FONDEN Investigator grant (project number 16599). RW thanks Luca Izzo, Darach Watson, Nandita Khetan, Christa Gall and Charlotte Angus for inspiring discussions. The authors thank the referee for insightful comments.

DATA AVAILABILITY

No new data were generated or analysed in support of this research.

REFERENCES

- Andersen P., Hjorth J., 2018, MNRAS, 480, 68
 Arnett W. D., 1982, ApJ, 253, 785
 Betoule M. et al., 2014, A&A, 568, A22
 Brout D., Scolnic D., 2021, ApJ, 909, 26
 Brout D. et al., 2022a, ApJ, 938, 110
 Brout D. et al., 2022b, ApJ, 938, 111
 Bulla M., Goobar A., Dhawan S., 2018, MNRAS, 479, 3663
 Burns C. R. et al., 2014, ApJ, 789, 32
 Carr A., Davis T. M., Scolnic D., Said K., Brout D., Peterson E. R., Kessler R., 2022, PASA, 39, e046
 Carrick J., Turnbull S. J., Lavaux G., Hudson M. J., 2015, MNRAS, 450, 317
 Cikota A., Deustua S., Marleau F., 2016, ApJ, 819, 152
 de Vaucouleurs G., 1974, in The Formation and Dynamics of Galaxies, Shakeshaft J. R., ed., Vol. 58, p. 1
 Dhawan S. et al., 2022, MNRAS, 510, 2228
 Draine B. T., 2003, ARA&A, 41, 241
 Finkelman I. et al., 2010, MNRAS, 409, 727
 Fitzpatrick E. L., 1999, PASP, 111, 63
 Fitzpatrick E. L., Massa D., 2007, ApJ, 663, 320
 Foley R. J. et al., 2018, MNRAS, 475, 193
 Foreman-Mackey D., Hogg D. W., Lang D., Goodman J., 2013, PASP, 125, 306
 Freedman W. L. et al., 2019, ApJ, 882, 34
 Goobar A., 2008, ApJ, 686, L103
 Hicken M. et al., 2009, ApJ, 700, 331

- Jones D. O. et al., 2019, *ApJ*, 881, 19
Kasen D., Woosley S. E., 2007, *ApJ*, 656, 661
Kauffmann G. et al., 2003, *MNRAS*, 341, 54
Kelly P. L., Hicken M., Burke D. L., Mandel K. S., Kirshner R. P., 2010, *ApJ*, 715, 743
Larison C., Jha S. W., Kwok L. A., Camacho-Neves Y., 2023, arXiv e-prints, arXiv:2306.01088
Legnardi M. V. et al., 2023, *MNRAS*, 522, 367
Livio M., Mazzali P., 2018, *Phys. Rep.*, 736, 1
LSST Science Collaboration et al., 2009, ArXiv e-prints, 0912.0201
Maguire K. et al., 2013, *MNRAS*, 436, 222
Mandel K. S., Scolnic D. M., Shariff H., Foley R. J., Kirshner R. P., 2017, *ApJ*, 842, 93
Mandel K. S., Thorp S., Narayan G., Friedman A. S., Avelino A., 2022, *MNRAS*, 510, 3939
Mannucci F., Della Valle M., Panagia N., 2006, *MNRAS*, 370, 773
Maoz D., Mannucci F., Nelemans G., 2014, *ARA&A*, 52, 107
Nicolas N. et al., 2021, *A&A*, 649, A74
Nobili S., Goobar A., 2008, *A&A*, 487, 19
Perlmutter S. et al., 1999, *ApJ*, 517, 565
Phillips M. M., Lira P., Suntzeff N. B., Schommer R. A., Hamuy M., Maza J., 1999, *AJ*, 118, 1766
Phillips M. M. et al., 2013, *ApJ*, 779, 38
Planck Collaboration et al., 2020, *A&A*, 641, A6
Popovic B., Brout D., Kessler R., Scolnic D., 2021, arXiv e-prints, arXiv:2112.04456
Pruzhinskaya M. V., Novinskaya A. K., Pauna N., Rosnet P., 2020, *MNRAS*, 499, 5121
Riess A. G., Casertano S., Yuan W., Bowers J. B., Macri L., Zinn J. C., Scolnic D., 2021, *ApJ*, 908, L6
Riess A. G., Casertano S., Yuan W., Macri L. M., Scolnic D., 2019, *ApJ*, 876, 85
Riess A. G. et al., 1998, *AJ*, 116, 1009
Riess A. G. et al., 2016, *ApJ*, 826, 56
Riess A. G. et al., 2022, *ApJ*, 934, L7
Rigault M. et al., 2020, *A&A*, 644, A176
Rigault M. et al., 2013, *A&A*, 560, A66
Rodney S. A. et al., 2014, *AJ*, 148, 13
Scalzo R. et al., 2014a, *MNRAS*, 440, 1498
Scalzo R. A., Ruiters A. J., Sim S. A., 2014b, *MNRAS*, 445, 2535
Scannapieco E., Bildsten L., 2005, *ApJ*, 629, L85
Schlafly E. F. et al., 2016, *ApJ*, 821, 78
Scolnic D. et al., 2015, *ApJ*, 815, 117
Scolnic D., Kessler R., 2016, *ApJ*, 822, L35
Scolnic D. M. et al., 2018, *ApJ*, 859, 101
Smith M. et al., 2020, *MNRAS*, 494, 4426
Sullivan M. et al., 2006, *ApJ*, 648, 868
Thorp S., Mandel K. S., Jones D. O., Ward S. M., Narayan G., 2021, *MNRAS*, 508, 4310
Tripp R., 1998, *A&A*, 331, 815
Uddin S. A. et al., 2020, *ApJ*, 901, 143
Wang K. X. et al., 2022, arXiv e-prints, arXiv:2204.13553
Wang X. et al., 2008, *ApJ*, 675, 626
Wiseman P. et al., 2022, *MNRAS*, 515, 4587
Wojtak R., Hjorth J., 2022, *MNRAS*, 515, 2790

APPENDIX A: POSTERIOR PROBABILITY

The probability of observing type Ia supernova with light curve parameters $\boldsymbol{\xi} = \{m_B, x_1, c\}$ measured with the covariance matrix \mathbf{C}_{obs} , a set of latent variables $\boldsymbol{\phi}$ drawn from two distinct supernova populations with relative fractions described by the weight parameter $0 < w < 1$ is given by

$$p(\{\boldsymbol{\xi}, \boldsymbol{\phi}\}) = w\mathcal{G}[\mathbf{d}; \boldsymbol{\xi}(\boldsymbol{\phi}), \mathbf{C}_{\text{obs}}]p_{\text{prior}1}(\boldsymbol{\phi}) + (1-w)\mathcal{G}[\mathbf{d}; \boldsymbol{\xi}(\boldsymbol{\phi}), \mathbf{C}_{\text{obs}}]p_{\text{prior}2}(\boldsymbol{\phi}), \quad (\text{A1})$$

where $\mathcal{G}(\mathbf{x}; \mathbf{a}, \mathcal{A})$ is a multivariate normal distribution with mean \mathbf{a} and covariance \mathcal{A} , $p_{\text{prior}i}(\boldsymbol{\phi})$ are prior distributions of latent variables in the two supernova populations ($i = 1, 2$). The predicted light parameters are related to the latent variables describing intrinsic supernova properties (absolute luminosity M_B , stretch-related parameter X_1 , intrinsic colour c_{int}), extrinsic properties of dust in supernova host galaxy (dust reddening $E(B-V)_i$ and extinction coefficient R_{B_i}), distance modulus μ in the following way:

$$\boldsymbol{\xi} = \begin{bmatrix} M_B + \mu - \alpha X_1 + \beta c_{\text{int}} + R_B E(B-V) \\ X_1 \\ c_{\text{int}} + E(B-V) \end{bmatrix}. \quad (\text{A2})$$

Adopting Gaussian priors for supernova intrinsic properties, the extinction coefficient and the distance modulus, i.e.

$$\begin{aligned} p_{\text{prior}i}(M_B) &= \mathcal{G}(M_B; \widehat{M}_{B_i}, \sigma_{M_B i}) \\ p_{\text{prior}i}(X_1) &= \mathcal{G}(X_1; \widehat{x}_{1_i}, \sigma_{x_1 i}) \\ p_{\text{prior}i}(c_{\text{int}}) &= \mathcal{G}(c_{\text{int}}; \widehat{c}_{\text{int}i}, \sigma_{c_{\text{int}i}}) \\ p_{\text{prior}i}(R_B) &= \mathcal{G}(R_B; \widehat{R}_{B_i}, \sigma_{R_B i}) \\ p_{\text{prior}i}(\mu) &= \mathcal{G}(\mu; \widehat{\mu}, \sigma_{\mu}), \end{aligned} \quad (\text{A3})$$

and delta distribution for parameters α_i and β_i , i.e. $\delta(\alpha_i)$ and $\delta(\beta_i)$, the posterior probability distribution for hyperparameters $\boldsymbol{\Theta}$ and parameter w can be simplified to the following form

$$\begin{aligned} p(\{\boldsymbol{\Theta}, w\} | \boldsymbol{\xi}_{\text{obs}}) &= \int_0^\infty w \mathcal{G}[\boldsymbol{\xi}_1(\boldsymbol{\Theta}, y_1); \boldsymbol{\xi}_{\text{obs}}, \mathbf{C}_1(\boldsymbol{\Theta}, y_1)] p_{\text{prior}1}(y_1 = E(B-V)_1/\tau_1) dy_1 + \\ &\int_0^\infty (1-w) \mathcal{G}[\boldsymbol{\xi}_2(\boldsymbol{\Theta}, y_2); \boldsymbol{\xi}_{\text{obs}}, \mathbf{C}_2(\boldsymbol{\Theta}, y_2)] p_{\text{prior}2}(y_2 = E(B-V)_2/\tau_2) dy_2, \end{aligned} \quad (\text{A4})$$

where $\{\tau_1, \tau_2\}$ are the scales of $E(B-V)$ distributions in host galaxies of the two supernova populations,

$$\boldsymbol{\xi}_i = \begin{bmatrix} \widehat{M}_{B_i} + \widehat{\mu} - \alpha_i \widehat{x}_{1_i} + \beta_i \widehat{c}_{\text{int}i} + \widehat{R}_{B_i} \tau_i y_i \\ \widehat{x}_{1_i} \\ \widehat{c}_{\text{int}i} + \tau_i y_i \end{bmatrix}, \quad (\text{A5})$$

and

$$\mathbf{C}_i = \mathbf{C}_{\text{obs}} + \begin{bmatrix} (\sigma_{\text{int}i}^2 + \sigma_{\mu}^2 + \alpha_i^2 \sigma_{x_1 i}^2 + \beta_i^2 \sigma_{c_{\text{int}i}}^2 + y_i^2 \tau_i^2 \sigma_{R_B i}^2) & -\alpha_i \sigma_{x_1 i}^2 & \beta_i \sigma_{c_{\text{int}i}}^2 \\ -\alpha_i \sigma_{x_1 i}^2 & \sigma_{x_1 i}^2 & 0 \\ \beta_i \sigma_{c_{\text{int}i}}^2 & 0 & \sigma_{c_{\text{int}i}}^2 \end{bmatrix}. \quad (\text{A6})$$

For the probability distribution of $E(B-V)$ used in this study, i.e.

$$p_{\text{prior}i}(y_i = E(B-V)/\tau_i) = \frac{y_i^{\gamma-1} \exp(-y_i)}{\Gamma(\gamma)}, \quad (\text{A7})$$

where γ is a shape parameter and $\Gamma(x)$ is the gamma function, the integrals in eq. (A4) are calculated numerically. The prior probability distribution is truncated at $y_{\text{max}i} = E(B-V)/\tau_i = 10$ and renormalized accordingly. The posterior probability for the entire sample of supernovae is then given by

$$p(\{\boldsymbol{\Theta}, w\} | \{\boldsymbol{\xi}_1, \dots, \boldsymbol{\xi}_N\}) = \prod_{j=1}^N p(\{\boldsymbol{\Theta}, w\} | \boldsymbol{\xi}_j). \quad (\text{A8})$$

For the analysis of the cosmological sample we use distance modulus $\widehat{\mu}_j$ given by the Planck cosmological model at supernova CMB rest frame redshift z_j . With peculiar velocities as the main source of uncertainties in distances moduli we also use

$$\sigma_{\mu j} = \frac{5}{\ln 10} \frac{\sigma_v}{c} \frac{1}{z_j} \quad (\text{A9})$$

with $\sigma_v = 250 \text{ km s}^{-1}$ equal to an upper limit of scatter in peculiar velocities with respect to the linear velocity field (Carrick et al. 2015).

supernova sample	SuperCal (156 SNe) 0.023 < z < 0.15		Pantheon+ light curve parameters (156 SNe) 0.023 < z < 0.15	
	SNe(pop1) fast declining	SNe(pop2) slowly declining	SNe(pop1) fast declining	SNe(pop2) slowly declining
\widehat{M}_B	$-19.42^{+0.08}_{-0.08}$	$-19.47^{+0.08}_{-0.09}$	$-19.48^{+0.12}_{-0.11}$	$-19.41^{+0.11}_{-0.13}$
\widehat{x}_1	$-1.08^{+0.47}_{-0.48}$	$0.50^{+0.19}_{-0.19}$	$-1.22^{+0.31}_{-0.26}$	$0.42^{+0.11}_{-0.11}$
σ_{x_1}	$0.80^{+0.24}_{-0.25}$	$0.55^{+0.16}_{-0.16}$	$0.70^{+0.21}_{-0.16}$	$0.60^{+0.08}_{-0.08}$
\widehat{c}_{int}	$-0.052^{+0.041}_{-0.043}$	$-0.111^{+0.040}_{-0.041}$	$-0.101^{+0.045}_{-0.042}$	$-0.132^{+0.042}_{-0.041}$
$\sigma_{c_{\text{int}}}$	$0.060^{+0.017}_{-0.018}$	$0.047^{+0.015}_{-0.016}$	$0.038^{+0.028}_{-0.028}$	$0.037^{+0.018}_{-0.019}$
τ	$0.022^{+0.011}_{-0.012}$	$0.033^{+0.009}_{-0.010}$	$0.041^{+0.013}_{-0.014}$	$0.041^{+0.010}_{-0.009}$
α		$-0.162^{+0.025}_{-0.027}$		$-0.196^{+0.029}_{-0.026}$
β		$3.052^{+0.332}_{-0.341}$		$2.414^{+0.559}_{-0.687}$
\widehat{R}_B	$3.57^{+1.19}_{-1.01}$	$4.71^{+0.83}_{-0.74}$	$3.09^{+0.46}_{-0.52}$	$3.69^{+0.59}_{-0.54}$
σ_{R_B}		$0.892^{+0.362}_{-0.328}$		$0.636^{+0.216}_{-0.204}$
γ		$3.429^{+1.422}_{-1.439}$		$3.106^{+1.295}_{-1.341}$
w		$0.474^{+0.204}_{-0.196}$		$0.380^{+0.102}_{-0.102}$

Table B1. Comparison between best fit model parameters derived from the original *SuperCal* supernova sample (left) and its analog with redshifts and light curve parameters updated from the *Patheon+* compilation (right). The adopted model allows for independent mean extinction coefficient \widehat{R}_B in the two supernova populations. Best fit results are provided as the posterior mean values and errors of the credibility range containing 68 per cent of the marginalised probabilities (or 68 per cent upper limits).

APPENDIX B: RESULTS FOR PANTHEON+ LIGHT CURVE PARAMETERS

Table B1 compares best fit parameters of the baseline model with independent \widehat{R}_B in both supernova populations obtained from the original *SuperCal* supernova sample (left) and its analog with redshifts and light curve parameters updated from the *Patheon+* compilation (Brout et al. 2022a). Figure B1 shows marginalised posterior distributions for the *Patheon+* data.

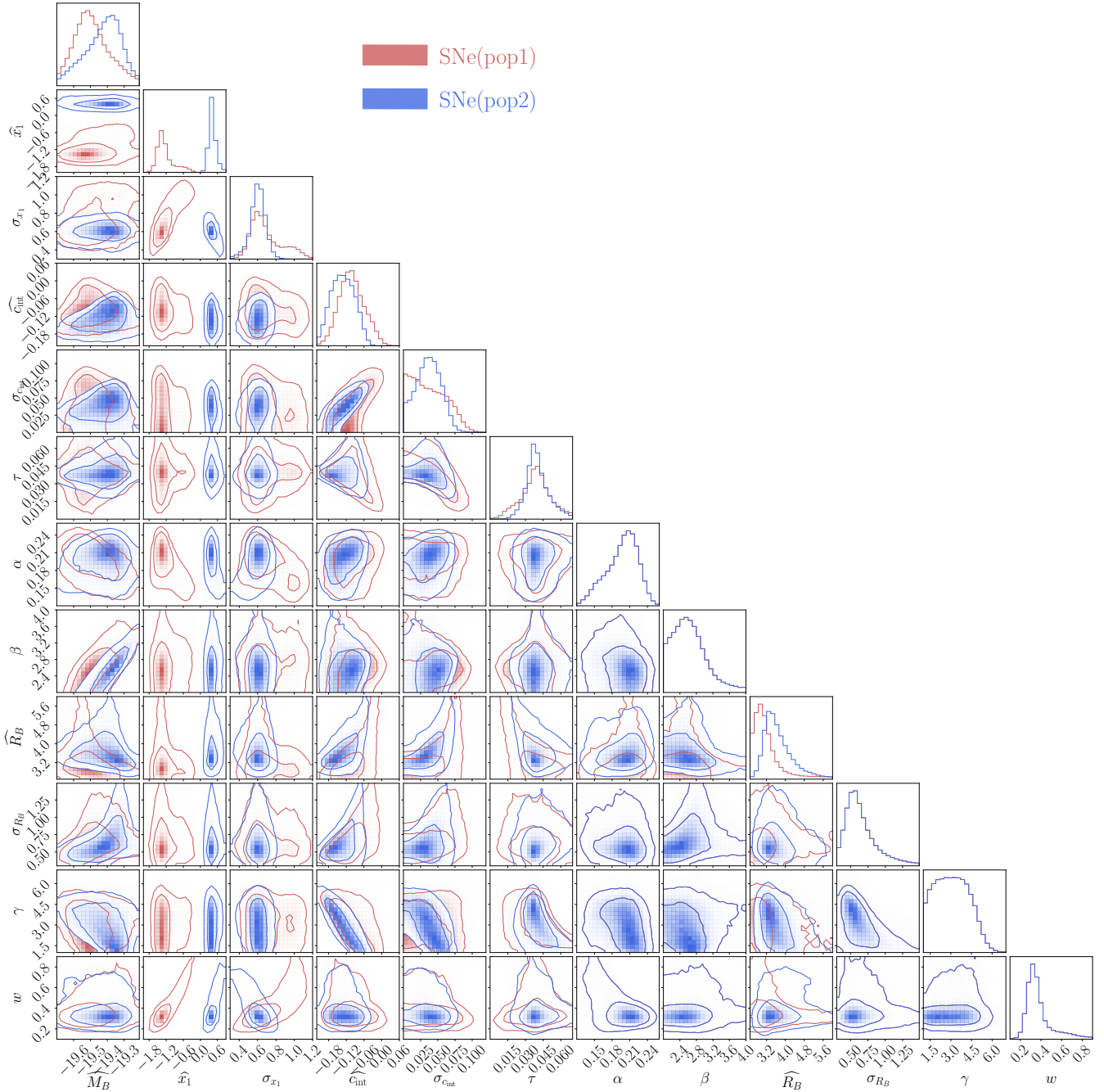


Figure B1. Constraints on hyperparameters of a one-parameter extension of the baseline model (independent mean extinction parameter in both supernova populations) obtained for the main *SuperCal* supernova sample with light curve parameters and redshifts updated from the *Pantheon+* catalogue. The red and blue contours show constraints on parameters in the two supernova populations: population 1 (fast declining supernovae, red) and population 2 (slowly declining supernovae, blue). For the sake of readability, the corner plot is compressed by overlaying the panels with the corresponding sets of hyperparameters. The contours show 1σ and 2σ confidence regions containing 68 and 95 per cent of 2-dimensional marginalised probability distributions.